C P No. 78
(13 786)
A.R.C. Technical Report

MINISTRY OF SUPPLY

AERONAUTICAL RESEARCH COUNCIL

CURRENT PAPERS

High Speed Wind Tunnel Tests on an Aerofoil with and without Two-dimensional Spanwise Bulges

By

J. A Beavan, M. A, and E. W. E Rogers, D.I.C, B.Sc,
of the Aerodynamics Division, N.P.L.
and
R. Cartwright, B E.,
of the Department of Supply, Australia

LONDON: HER MAJESTY'S STATIONERY OFFICE

1952

FIVE SHILLINGS NET.

C.P. No. 78

High Speed Wind Tunnel Tests on an Aerofoil with and without Two-Dimensional Spanwise Bulges.

- By -
J. A. Beavan, M.A., and E. W. E. Rogers, D.I.C., B.Sc.,
of the Aerodynamics Division, N.P.L.
- and -
R. Cartwright+ B.E.,
of the Department of Supply, Australia.

16th February, 1951

Summary

Results from high-speed wind-tunnel tests on a 5 inch chord pressure-plotting aerofoil having a single spanwise bulge on each surface have been compared with those obtained from the plain aerofoil (R.A.E.104 section; t/c = 0.10). The comparison has been made at five incidences (0°, $\pm 2^\circ$, $\pm 4^\circ$) for a limited range of Mach number; the test Reynolds number was between 1.5 and 1.9 million.

One bulge had a maximum height of 0.004 chord and extended from 0.3 to 0.5 chord. The other bulge was half of both these dimensions. The experimental pressure distributions at low speeds for both surfaces agree with those predicted by theory. The C_L is generally greater than for the plain aerofoil, but the corresponding changes in C_m are small except at the higher speeds.

At low speeds and zero incidence, boundary layer transition took place at about the bulge centres (0.4 chord) compared with 0.75 chord for the plain aerofoil; the resulting increase in C_D agrees with theory. With increase in Mach number an initial rise in drag (due to shock waves on the bulge) occurs at both 0° and 2° incidence. This rise is halted as the main shock wave and transition point move back and the final drag rise takes place at about the same Mach number as on the plain aerofoil.

The shock pattern is considerably modified by the presence of the bulges, the waves being stronger and more well-defined than on the plain aerofoil. This is due to the higher local Mach number achieved ahead of the shock in the former case.

Contents/

+At present attached to the Aerodynamics Division, N.P.L.

Published by permission of the Director, National Physical Laboratory.

1./

1. Introduction

In flight tests at high speeds, interpretation of results is often in doubt due to distortion of wing surfaces under high loading. Similarly, uncertainties arise in high-speed tunnel tests where models may sometimes have inaccuracies of the order of 0.2% chord (0.02 inches on 12 inches chord). Little is known as to the effect on shockwave development of such bulging as may occur, the chief work from the U.S.A.[1], and Germany[2] being on particular configurations of "wrinkles" related to actual measured distortions on full-scale aircraft. The following tests with a single bulge on each surface were carried out in the hope of obtaining information leading to more general conclusions.

2. Model

A series of tests has been made in the N.P.L. 20 in.× 8 in. High Speed Wind Tunnel on a two-dimensional five-inch chord pressure plotting aerofoil of RAE 104 section and 10% thickness/chord ratio. This section (though with a slightly modified trailing edge) has already been tested on a balance in the R.A.E. High Speed Tunnel and was designated "H.S.7" in the report[3] on that work. It was found convenient to construct the N.P.L. model initially with bulges on both surfaces; these were later removed to allow comparison tests to be made.

It was decided to make the proportions of the bulges similar to those that may have occurred in flight, and to place them at 0.40 chord near the maximum thickness position (0.42 chord). On the assumption that effects on the two surfaces would be reasonably independent of each other, a single bulge was made on each side of the aerofoil, that on the upper surface being 0.004c high (0.02 inches on the 5 inch chord model) and approximately 0.20c long, and that on the lower surface being half of these dimensions. Fuller details are given in Figure 1 and Tables I and II. These dimensions, according to the criterion given by Page in Reference 4, are sufficient to cause transition to take place on both bulges at the Reynolds number of the experiment (between 1.5 and 1.9 million).

3. Range of Tests

It was not desired to devote very much time in the tunnel to these measurements, so after a preliminary visual observation of the shockwave behaviour on the aerofoil with bulges, a restricted range of Mach number was chosen for five incidences, 0°, $\pm 2^\circ$, $\pm 4^\circ$. At low speeds and zero incidence the velocity on the bulge is considerably higher than elsewhere on the aerofoil; on the upper surface at 2° the velocity is only a little higher, and at 4° much lower, than that near the nose. Figure 2 illustrates these cases with experimental curves obtained at Mach numbers near 0.6.

At various Mach numbers direct-shadow photographs, wake traverses (to determine the drag) and surface pressure distributions were obtained; the last were extended over a wider and more detailed range of speed than were the other measurements. All the observations were repeated after the bulges had been removed.

The flexible walls of the tunnel were set to shapes, which in the absence of the model gave a constant pressure along their length (i.e., equivalent to straight walls with taper to allow for increasing boundary-layer thickness). In consequence the results have been corrected (for blockage only) on the basis of Ref.5.

4./

4. Presentation of Results

The measured pressure distributions for the aerofoil with bulges are given in Figures 3-6, in terms of the variable p/H_o, this being the ratio of the static pressure at the model surface to the stagnation pressure. Since there were not sufficient pressure holes to define the shape of the curve over the bulges, the theoretical low-speed distribution, calculated by the 40-point method in use at the N.P.L. and increased according to the Kármán-Tsien law, was used as a guide in linking up the experimental points. Figure 7 shows that with a slight rearward displacement, the theoretical curve fits the experimental points quite well.

Lift and pitching moment coefficients were obtained by integrating the pressure distribution curves and are plotted in Figures 11 and 12. Figure 13 shows the variation of drag coefficient with Mach number for the aerofoil with and without bulges, as obtained from total head traverses in the wake one chord length behind the trailing edge. Typical traverse curves for the aerofoil with bulges are shown in Figure 14.

Direct shadow photographs (obtained with a short duration spark as a light source) shewing the flow around the model in the two tests are reproduced in Figures 15 to 19, together with the corresponding pressure distribution curves. No special efforts were made to obtain high quality photographs; much of the field, particularly near the aerofoil surface, was obscured by supports and pressure leads+, but it was possible to watch the development of shock phenomena over the whole of the upper surface and to observe the boundary layer from about 45% chord, i.e., just behind the centre of the bulge. To increase the unobscured region on the lower surface at negative incidences, the pressure leads were sometimes brought out on the upper surface side as in Figure 18a. As with most of the tests in this tunnel the shocks often appear broad (or multiple) probably due to variation in flow over the eight inch span between the glass walls, or to interaction of the shockwave with the boundary layer on these walls.

5. Results and Discussion

(a) $\alpha = 0^\circ$

At this incidence the velocity peak over the bulges at sub-critical free-stream Mach numbers is much higher than at any other point on the aerofoil; thus critical conditions first arise in this region, sonic speed being reached locally at $M = 0.707$. Boundary layer transition takes place at the bulge instead of about 0.75 chord for the plain aerofoil. By $M = 0.751$ (Figure 15a) a well developed shockwave has formed just behind the bulge and the drag coefficient has risen somewhat above the low-speed value (Figure 13).

As/

+The aerofoil supports are outside the tunnel at right angles to the chord on the lower surface side; the rubber pressure leads (also outside the tunnel) are bunched together and brought forward usually on the same side of the model as the supports. Moreover protuberances on the upper surface, such as those seen in Figures 15a to 19a are not connected with the bulges on the aerofoil (which would be too small to be seen) but are clearance holes for the supporting pins in the glass of the tunnel side-walls.

As the tunnel speed is raised further, the main shock moves steadily back, taking with it the boundary layer transition point. A weak oblique shock from the top of the bulge meets the main shock some distance from the aerofoil surface; the inclined shock from the large bulge is the more diffused close to the aerofoil, although near the junction with the normal shock both inclined waves are well defined (Figure 15a). This difference may be due to the lower absolute surface curvature of the larger bulge. Figure 14 shows that there is an increase in total head loss in the region directly behind the intersection. By comparison, no well defined shockwave appears on the plain aerofoil even up to $M = 0.818$ although numerous wavelets are visible (the pressure critical Mach number at this incidence is 0.79).

The pressure distributions for the region ahead of the bulges exhibit only a small variation of the coefficient C_p over the whole speed range. Above $M = 0.80$ the local Mach number on the upper surface bulge and that just behind it remain roughly constant at about 1.3 and 1.2 respectively, even though at the highest tunnel speeds the local Mach number farther back (i.e., just ahead of the main shockwave) again reaches 1.3. (Figure 3). This reduction from $M = 1.3$ to $M = 1.2$ is presumably associated with the inclined shock.

The increase in the laminar flow region as the Mach number is raised, reduces the rate of drag rise until a free stream Mach number of about 0.80 is reached. Above this, there is a thickening of the boundary layer ahead of the base of the main shock, resulting in a widening of the wake centre and a further sharp rise in drag. (Figure 13).

A similar progression of events occurs on the lower surface but there are some minor differences due to the smaller size of the bump. The velocity increment is of the same magnitude on both bulges at sub-critical speeds although it extends less along the chord in the case of the smaller bulge. At the higher speeds its effect is less than that observed on the upper surface, a maximum Mach number of 1.2 being reached on the bulge[+]; at the highest speed of test a local Mach number of 1.3 is attained just ahead of the shock.

Up to about $M = 0.81$, transition occurs at about 0.75 chord on the plain aerofoil and the drag coefficient remains constant; at higher speeds development of the wave pattern and thickening of the boundary layer produces an increase in drag. The final drag rise occurs on each aerofoil at nearly the same speed. (Figure 13).

(b)/

[+]It is possible that a higher value of M is reached between the two pressure holes situated at 0.40 and 0.44 chord. This might be expected because of the inclination of the oblique shock which is 53° to the local free-stream direction at a free-stream Mach number of 0.80. Combined with the maximum deflection (4.1°) of the stream by the bulge, this would give a change in Mach number across the shock of 1.37 to 1.22. But the argument is weakened because at the corresponding position on the upper surface, a shock wave inclination of 46° would similarly be expected to give a change of from $M = 1.52$ to 1.37; this seems unlikely from the experimental results. It is possible that the discrepancy in the local reduction of Mach number may be due to a reduction of the stream deflection by a temporary laminar separation.

(b) $\alpha = +2^\circ$

On the upper surface at low speeds, the velocity peak near the nose is not as high as that on the bulge. Hence with the increase of free-stream velocity, the speed of sound is reached first at the bulge ($M = 0.66$ approximately) and later ($M = 0.705$) near the nose. The photographs (Figure 16a) suggest that a shock develops on the bulge at about $M = 0.70$ and also nearer the nose at $M = 0.769$, although diffuse wavelets are much in evidence at lower speeds. As the Mach number is increased the former shock moves rearward somewhat irregularly (Figure 20). But the more forward shock (which is well marked at $M = 0.769$ and moves back rapidly with increase of speed) disappears from the aerofoil surface by $M = 0.792$, as the mixed flow region on the surface ahead of the bulges is replaced by a smoothed supersonic region (Figure 4).

As far as can be judged, the boundary layer does not thicken forward of the base of the shock until the Mach number exceeds 0.769, and this is supported by evidence of the constancy of the wake width up to that speed. The pressure distribution curves suggest that boundary-layer separation does not take place at the trailing edge even up to the highest Mach number tested (0.792), the value of the coefficient C_p in this region, the trailing edge remaining reasonably constant.

As at 0°, and presumably for similar reasons, there is a step in the drag curve (Figure 13) at a free stream Mach number of about 0.76; the final drag rise occurs only a little earlier than on the plain aerofoil. For the latter model, the pressure critical Mach number is 0.717, and scattered wavelets are visible up to $M = 0.766$. At a higher speed ($M = 0.788$) the shockwave is strong enough to cause thickening of the boundary layer at its foot; this coincides with the beginning of the drag rise. Further, the pressure distribution changes in shape, that with a suction peak at the nose giving place to a distribution having a favourable pressure gradient back to about 35% chord at the highest test Mach number (0.788); the boundary layer in this case is laminar[8] back to the foot of the shock (0.5c).

(c) $\alpha = +4^\circ$

At this incidence, there is a considerable velocity peak at subcritical speeds close to the nose, of greater magnitude than that due to the bulge. In fact, with rising speed the critical pressure is reached on the nose well before $M = 0.6$ (the peaks are not well enough defined to enable a precise value to be obtained), and on the bulge at $M = 0.65$ (Figure 5). At the latter speed the photograph (Figure 7a) shows wavelets behind the bulge and a complex wave system near the nose (about 0.1c). At $M = 0.69$ strong normal waves exist at both 0.22c and also behind the bulge, but as at 2°, the more forward wave disappears suddenly in this case between $M = 0.711$ and $M = 0.717$ (the marked change in the pressure distribution curve is shown in Figure 5). At higher speeds there is a single shockwave which moves downstream with increase of free stream Mach number. The pressure changes associated with the shock movements lead to a lift/Mach number curve with a kink at about $M = 0.72$ (Figure 11); the decrease in C_m at the higher Mach numbers is also irregular. (Figure 12a).

Comparison of the wake traverse curves at $M = 0.69$ and $M = 0.717$ (Figure 14b) shows that the wake losses actually decrease between these speeds; this is due to the increase in the laminar flow region following the disappearance of the forward wave. However this is more than offset by the growth of the bulge shockwave, and the nett effect is an increase in drag coefficient. (Figure 13).

For/

For the plain aerofoil, once the critical Mach number ($M = 0.54$) has been exceeded, the suction peak near the nose gives place to a region of fairly low supersonic velocity ($M = 1.25$) which increases in extent as the shock moves back (Figure 20), although more slowly than when the bulges are present.

The shockwave reaches 0.4 chord position on the plain aerofoil at $M = 0.74$ and the corresponding condition with a single shock on the aerofoil with bulges occurs when $M = 0.717$. In the latter case the wave appears stronger and the drag rise, although not easy to define, seems to occur earlier. (Figure 13).

(d) Negative Incidences

Comparison of the results obtained at negative and positive incidences affords some information on the effects of bulge size. Figures 4 and 18 show that the development of the pressure distribution at -2° incidence is not very different from that at the positive incidence; the disappearance of the forward shock takes place at about $M = 0.765$ instead of $M = 0.775$. The step in the drag coefficient/Mach number curve was also observed at the negative angle. (Figure 13).

Similarly there is little difference in the general shock development at plus and minus four degrees (Figure 5) even when the shockwave has moved past the bulge. The kink in the lift curve (Figure 11) was not observed, although it may exist as shown dotted.

(e) Comparison of Force Coefficients

Figures 11, 12 and 13 present a comparison of the lift, quarter-chord pitching moment and drag coefficients for the aerofoil with and without bulges. In the former case the lift-curve slope is increased by about 6 percent at $M = 0.6$ and except at $\alpha = -4^\circ$, the lift coefficient is everywhere higher.

The disparity between the C_L curves for the plain aerofoil at $\pm 4^\circ$ is difficult to account for; the results were confirmed when repeated, but subsequent tests[6] in which the flexible walls of the tunnel were used to reduce interference and the tunnel speed hole changed to the opposite side of the tunnel for negative incidences, gave almost exact agreement between positive and negative angles. However, since the experimental method was similar for the two sets of tests described in the present report, lack of symmetry in the results at this angle is not felt to affect the general conclusions.

It is unfortunate that the limited Mach number range prevented the maximum lift coefficient for a given incidence being obtained; what evidence there is suggests that only its value and not the Mach number, at which it occurs is affected by the presence of the bulges (cf. $\alpha = -2^\circ$, Figure 11).

At low Mach numbers there is some similarity between the two sets of moment coefficient curves, the values of C_M at $M = 0.6$ are almost unaffected by the presence of the bulges. In general the sudden falling away of C_M with increasing Mach number occurs earlier and is more irregular for the aerofoil with bulges, this being due to the rapid irregular backward movement of the forward shock.

The/

The drag coefficient curves given in Figure 13 show that over the whole Mach number range the effect of the bulges is to increase the drag, the percentage increase at low Mach number being largest at zero incidence. At $M = 0.6$ and zero incidence the observed drag values agree well with those predicted from theory[7] if transition is assumed to take place at 40% and at 75% chord in each case. The position of the final drag rise at 0° and 2° appears to be unaffected by the bulges but at 4° it seems to occur later for the plain aerofoil. As far as can be judged the subsequent rate of drag rise is then much the same at all incidences, for both states of the model.

6. Concluding Remarks

(a) In conditions where the flow is everywhere subsonic, the effect of a bulge near the maximum thickness position is to produce a velocity increment at the surface. The increments observed in the present tests agree closely with those predicted by the theory; the absolute value of the lift coefficient is increased but changes of the pitching moment coefficient are small. Since the bulges used were of sufficient size to cause boundary-layer transition, the magnitude of the drag coefficients was increased from the values observed on the plain aerofoil. They remained however almost independent of Mach number throughout the subcritical flow region.

(b) In the case where sonic speed is reached on a bulge before it occurs elsewhere on the aerofoil surface, a shock first forms just behind the bulge and produces some increase in drag. Subsequently the bulge (in the local supersonic flow) no longer causes transition but gives rise only to an inclined wave within the supersonic region. Except for this inclined wave the presence of the bulges has little effect on the flow at higher Mach numbers, and the final drag rise position is unchanged.

(c) At incidences at which sonic speed is first reached ahead of the bulge there may be two normal shock waves on the aerofoil surface. The first shock subsequently disappears as the Mach number increases, and its disappearance causes large irregular changes of the pitching moment coefficient and small changes of the lift coefficient; the drag rise seems to occur earlier than on the plain aerofoil. In all cases the final drag rise is accompanied by thickening of the boundary layer ahead of the foot of the shockwave.

(d) The presence of bulges does not seem to affect the often-remarked inability of the surface velocity to increase beyond about $M = 1.45$, since the effect of the bulge in a supersonic region of flow is very much smaller than its effect in a subsonic flow. The maximum Mach number observed on the bulge was about 1.3.

The results show clearly the importance of accurate reproduction of profiles, particularly in comparison between flight and wind tunnel tests. It is obvious that the pressure distribution on an aerofoil with, say, three or four bulges of the present kind on each surface will bear little resemblance to that applicable to the "ideal shape".

Acknowledgement

The authors wish to acknowledge the assistance given by Mr. A. Marchant, B.Sc., and Miss P. Burrows in the initial stages of the experimental work and by Miss B. Davis who was responsible for most of the calculations involved in preparing the figures.

References/

References

No.	Author(s)	Title, etc.
1	H. L. Robinson	High-speed Investigation of Skin Wrinkles on Two N.A.C.A. Airfoils. N.A.C.A. T.N.1121.
2	T. Zobel and W. K. Ritter	Measurements on the Rectangular Wing of the He 177 with and without wrinkles in the High-speed Tunnel (2.8m) at L.F.A. Volkenrode Report and Translation 521. (April, 1943).
3	R. Hills and H. E. Gamble	Preliminary Note on Tests on Three 10% Thick Aerofoils (H.5,6,7,8) in the R.A.E. High Speed Tunnel. R.A.E. Tech. Note No. Aero.1926. (December, 1947). A.R.C.11,117
4	A. Fage	The Smallest Size of a Spanwise Surface Corrugation which Affects Boundary-layer Transition on an Aerofoil. (January, 1943). R.& M.2120.
5	J. S. Thompson	Present Methods of Applying Blockage Corrections in a Closed Rectagular High Speed Wind Tunnel. R.A.E.Report No.Aero 2225. (January, 1948). A.R.C.11,385
6	E. W. E. Rogers, C. J. Berry and R. F. Cash	Tests at High Subsonic Speeds on a 10% Thick Pressure-plotting Aerofoil of R.A.E.104 Section. Part I. Force Coefficients. (November, 1950). A.R.C.13509
7	N. E. Winterbottom and H. B. Squire	Note on further Wing Profile Drag Calculations. Addendum to R.& M.1838. R.A.E. Report No.B.A.1634. A.R.C.4871
8	H. H. Pearcy	The Indication of Boundary Layer Transition on Aerofoils in the N.P.L. 20in × 8in. High Speed Wind Tunnel. Current Paper No.10. (December, 1948).

TABLE I

Ordinates of Main Aerofoil and additional Increment due to Bulges

x/c	y/c	x/c	y/c	Increment due to Bulge η/c — Upper Surface	Increment due to Bulge η/c — Lower Surface	x/c	y/c
0	0	0.10	0.03234			0.56	0.04584
0.001	0.00340	0.12	0.03500			0.60	0.04466
0.002	0.00484	0.14	0.03720			0.62	0.04324
0.003	0.00594	0.16	0.03920			0.64	0.04142
0.004	0.00688	0.18	0.04100			0.66	0.03960
0.005	0.00770	0.20	0.04258			0.68	0.03760
0.006	0.00844	0.22	0.04394			0.70	0.03534
0.007	0.00910	0.24	0.04514			0.72	0.03320
0.008	0.00970	0.26	0.04618			0.74	0.03100
0.010	0.01084	0.28	0.04708			0.76	0.02880
0.012	0.01184	0.30	0.04790	0.00005		0.78	0.02640
0.014	0.01276	0.32	0.04860	0.00025		0.80	0.02382
0.016	0.01366	0.34	0.04920	0.00084	0.00002	0.82	0.02148
0.018	0.01448	0.36	0.04950	0.00200	0.00042	0.84	0.01912
0.020	0.01526	0.38	0.04970	0.00336	0.00100	0.86	0.01678
0.025	0.01708	0.40	0.04990	0.00400	0.00200	0.88	0.01442
0.030	0.01864	0.42	0.05000	0.00336	0.00100	0.90	0.01208
0.035	0.02006	0.44	0.04990	0.00200	0.00042	0.92	0.00972
0.04	0.02136	0.46	0.04980	0.00084	0.00002	0.94	0.00738
0.05	0.02366	0.48	0.04940	0.00025		0.96	0.00502
0 06	0.02574	0.50	0.04900	0.00005		0.98	0.00268
0.07	0.02760	0.52	0.04860			1.00	0.00032
0.08	0.02948	0.54	0.04780				
0.09	0.03084	0.56	0.04702				

Equations for (η/c)

Upper Surface

$$\eta/c = 0.004\left(\frac{1}{2}\right)^{\left[25(0.40 - x/c)\right]^2}$$

Lower Surface

$$\eta/c = 0.002\left(\frac{1}{2}\right)^{\left[50(0.40 - x/c)\right]^2}$$

TABLE II/

TABLE II

(a) Pressure Hole positions for aerofoil with bulges (chord 5.05in

Hole Number	x/c position		Hole Number	x/c position	
	Upper Surface.	Lower Surface.		Upper Surface.	Lower Surface.
L.E.	0	-	9	0.436	0.555
1	0.002	0.005	10	0.495	0.614
2	0.010	0.059	11	0.555	0.673
3	0.040	0.158	12	0.614	0.733
4	0.099	0.297	13	0.673	0.822
5	0.198	0.356	14	0.733	0.941
6	0.297	0.396	15	0.792	
7	0.356	0.436	16	0.871	
8	0.396	0.495	17	0.941	

TABLE II

(b) Pressure Hole Positions for plain aerofoil (chord 5.06in

Hole Number	x/c position		Hole Number	x/c position	
	Upper Surface.	Lower Surface.		Upper Surface.	Lower Surface.
L.E	0	-	9	0.44	0.56
1	0.002	0.005	10	0.50	0.62
2	0.01	0.02	11	0.56	0.68
3	0.04	0.10	12	0.62	0.74
4	0.10	0.16	13	0.68	0.83
5	0.16	0.26	14	0.74	0.95
6	0.23	0.36	15	0.80	
7	0.30	0.44	16	0.88	
8	0.36	0.50	17	0.95	

JDS.

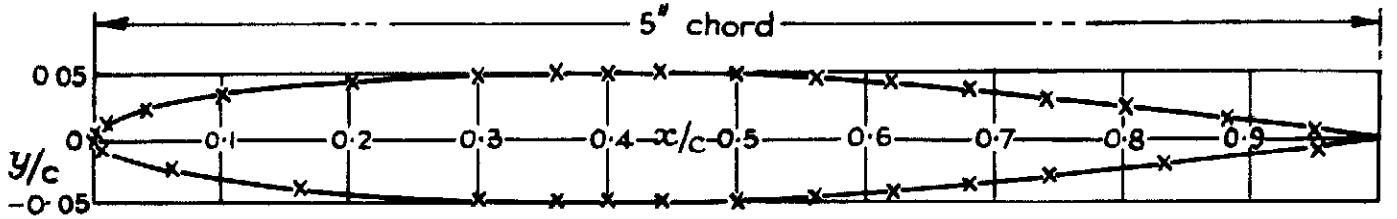

(a) Plain Aerofoil Profile showing original disposition of pressure-holes.

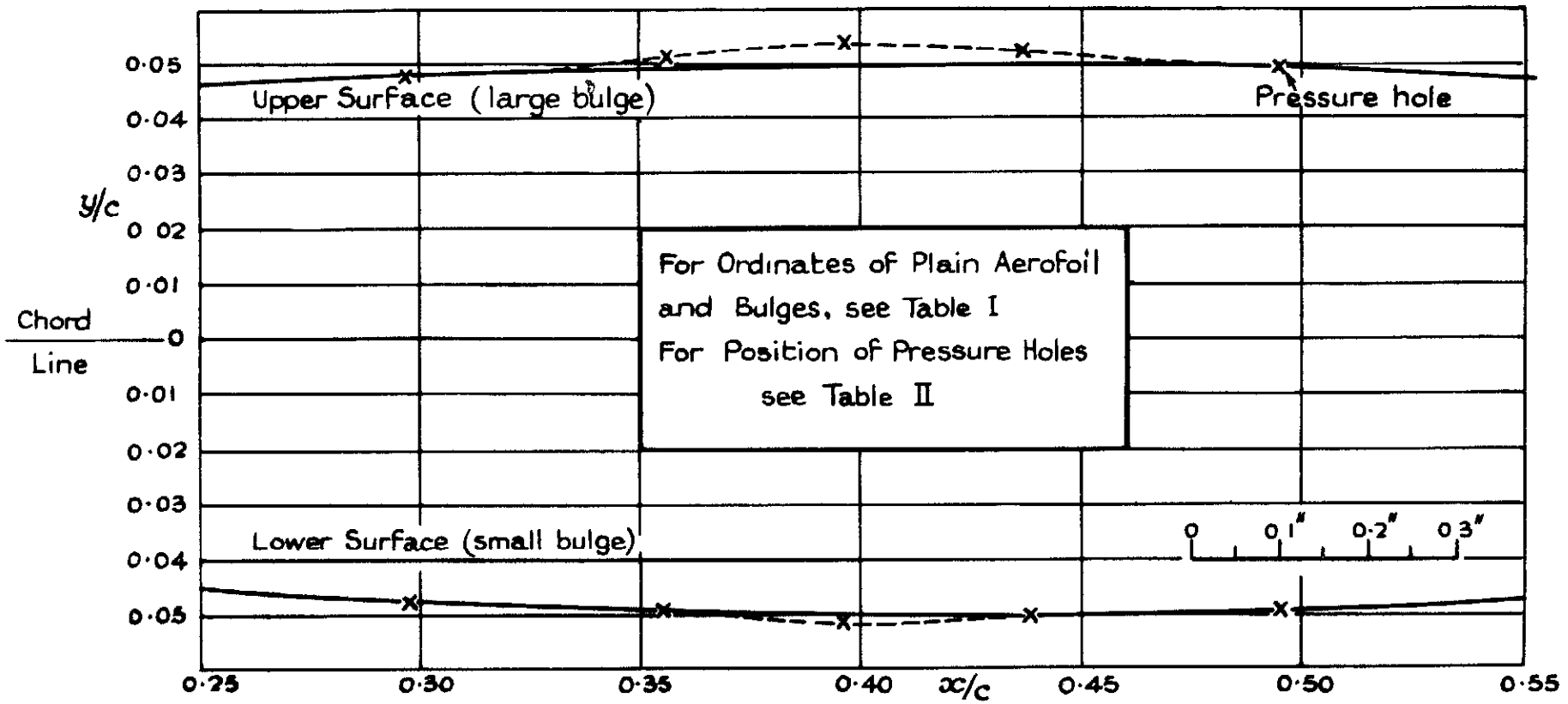

(b) Aerofoil Profile in region of Bulges

13,786.
FIG. 1.

E.R.M.

FIG. 2.

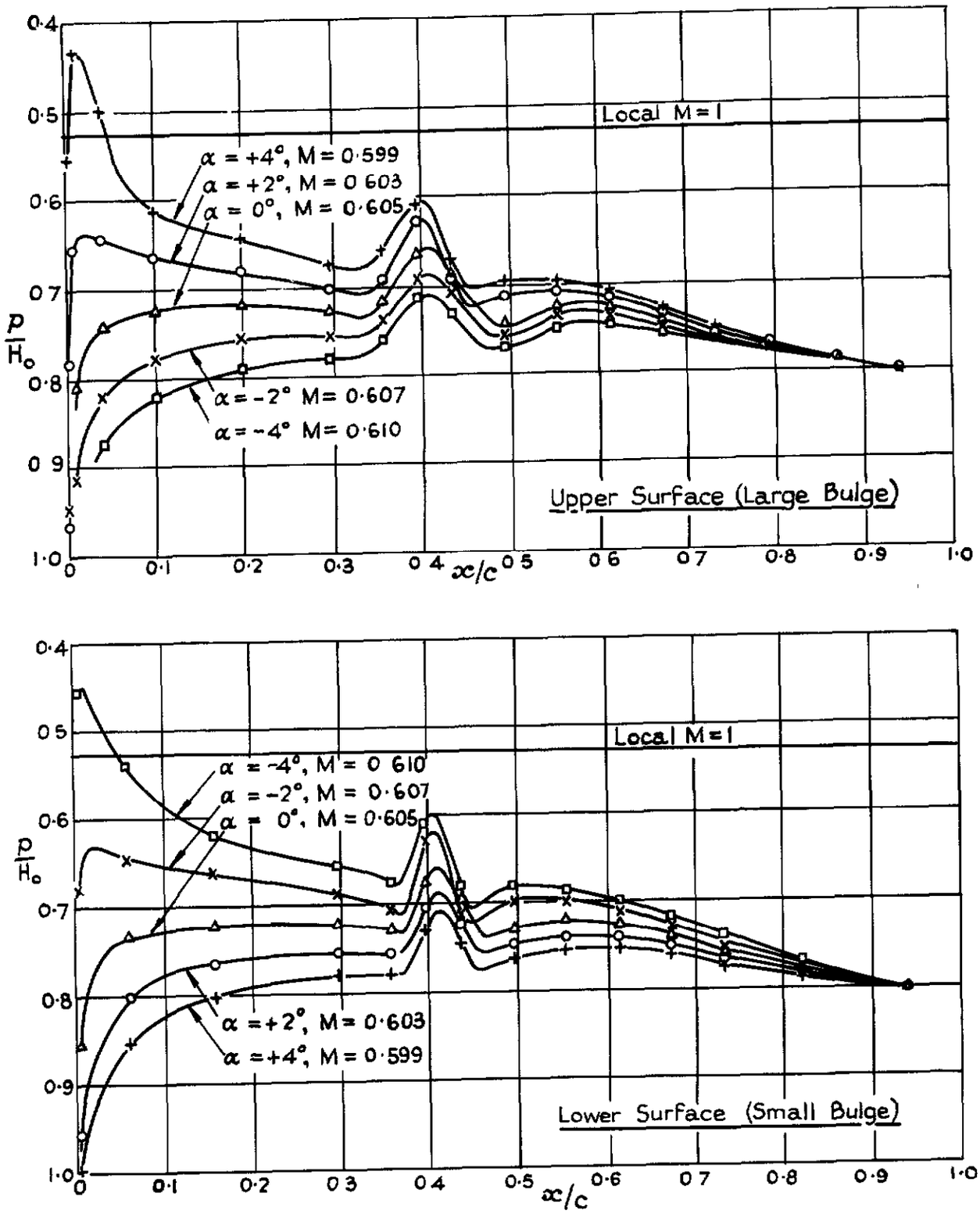

Measured Pressure Distributions at M ≃ 0·6 on Aerofoil with Bulges

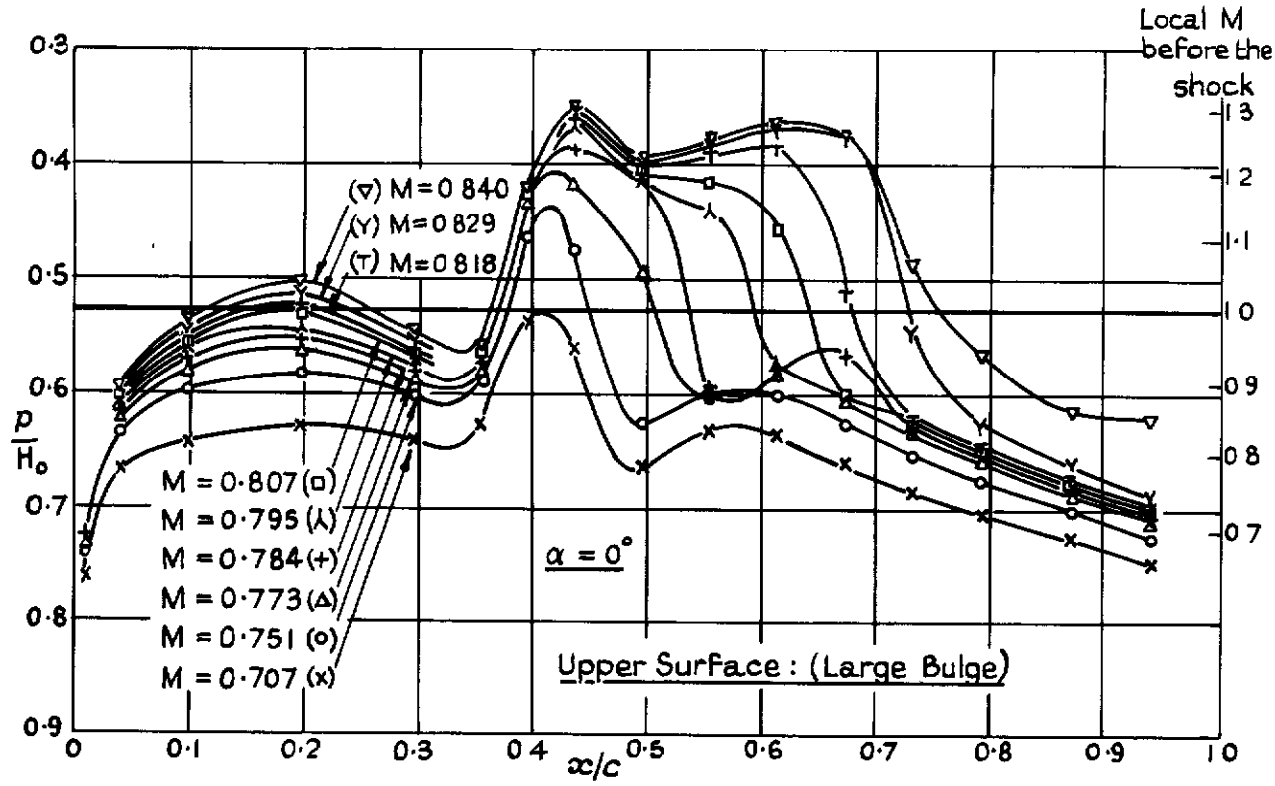

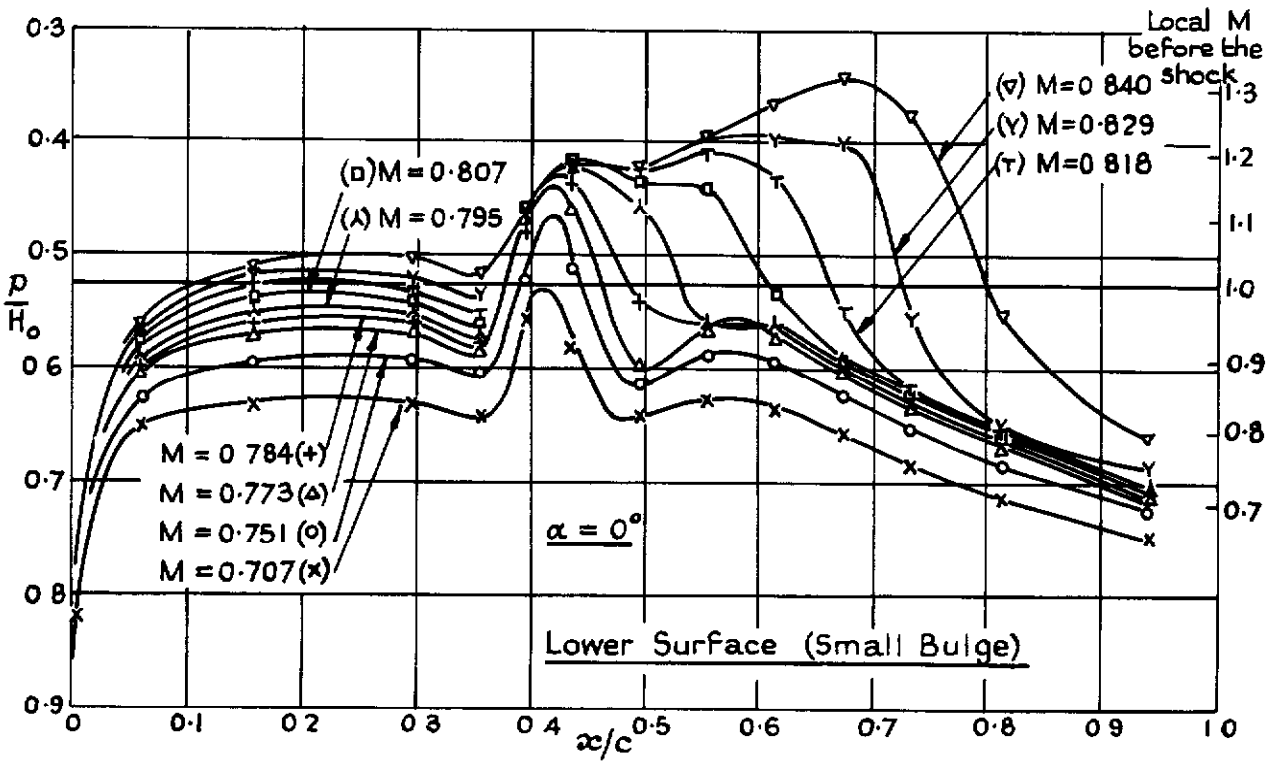

Pressure Distributions for Aerofoil with Bulges. $\alpha = 0°$

EEM

FIG 4

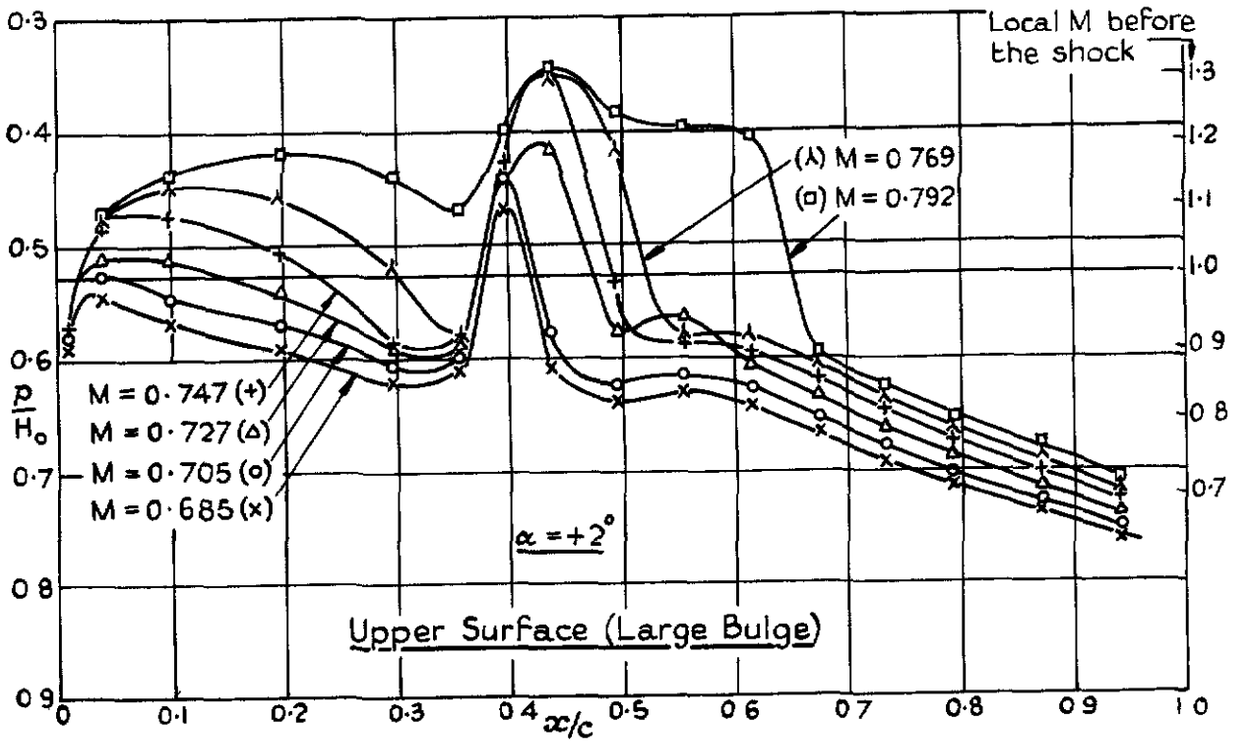

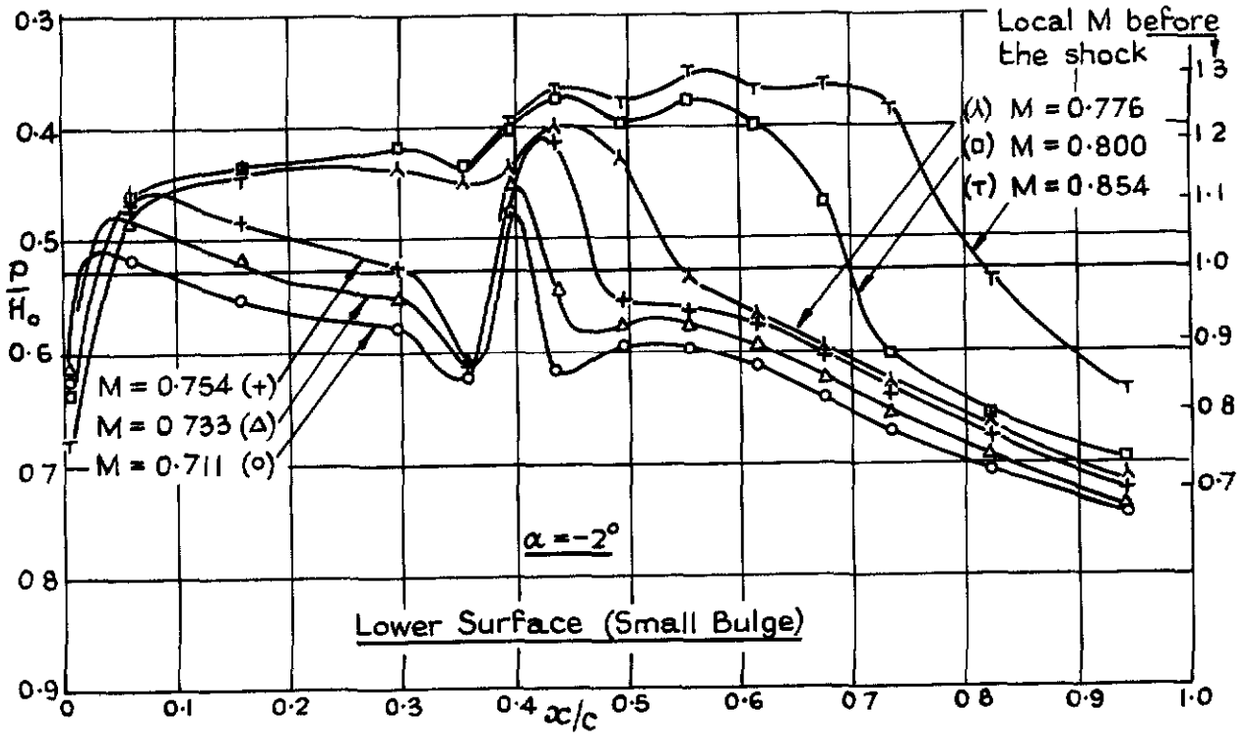

Pressure Distributions for Aerofoil with Bulges: $\alpha = +2$ & $-2°$

EEM

FIG 5.

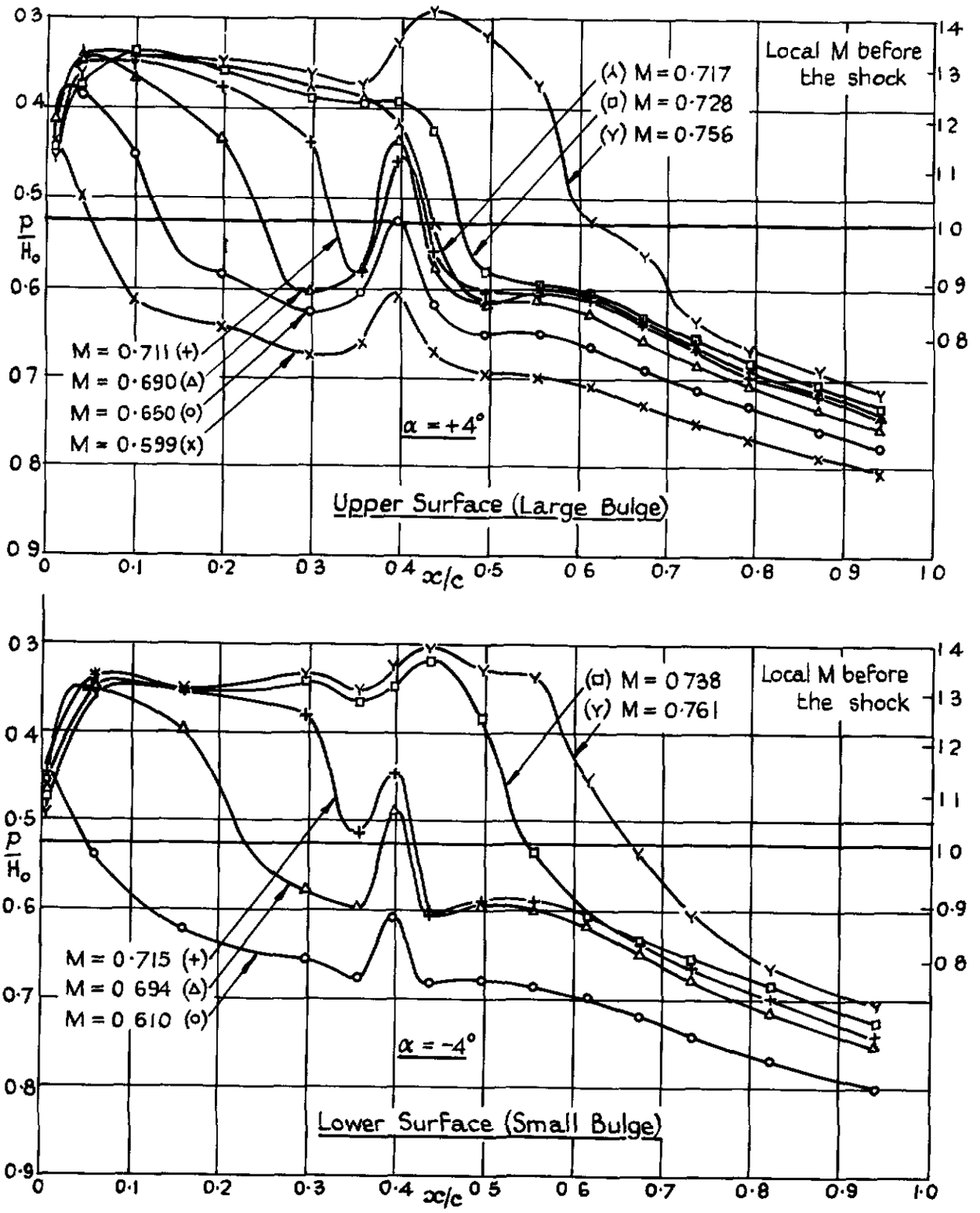

Pressure Distributions for Aerofoil with Bulges: $\alpha = +4° \& -4°$

E.E.M

FIG 6.

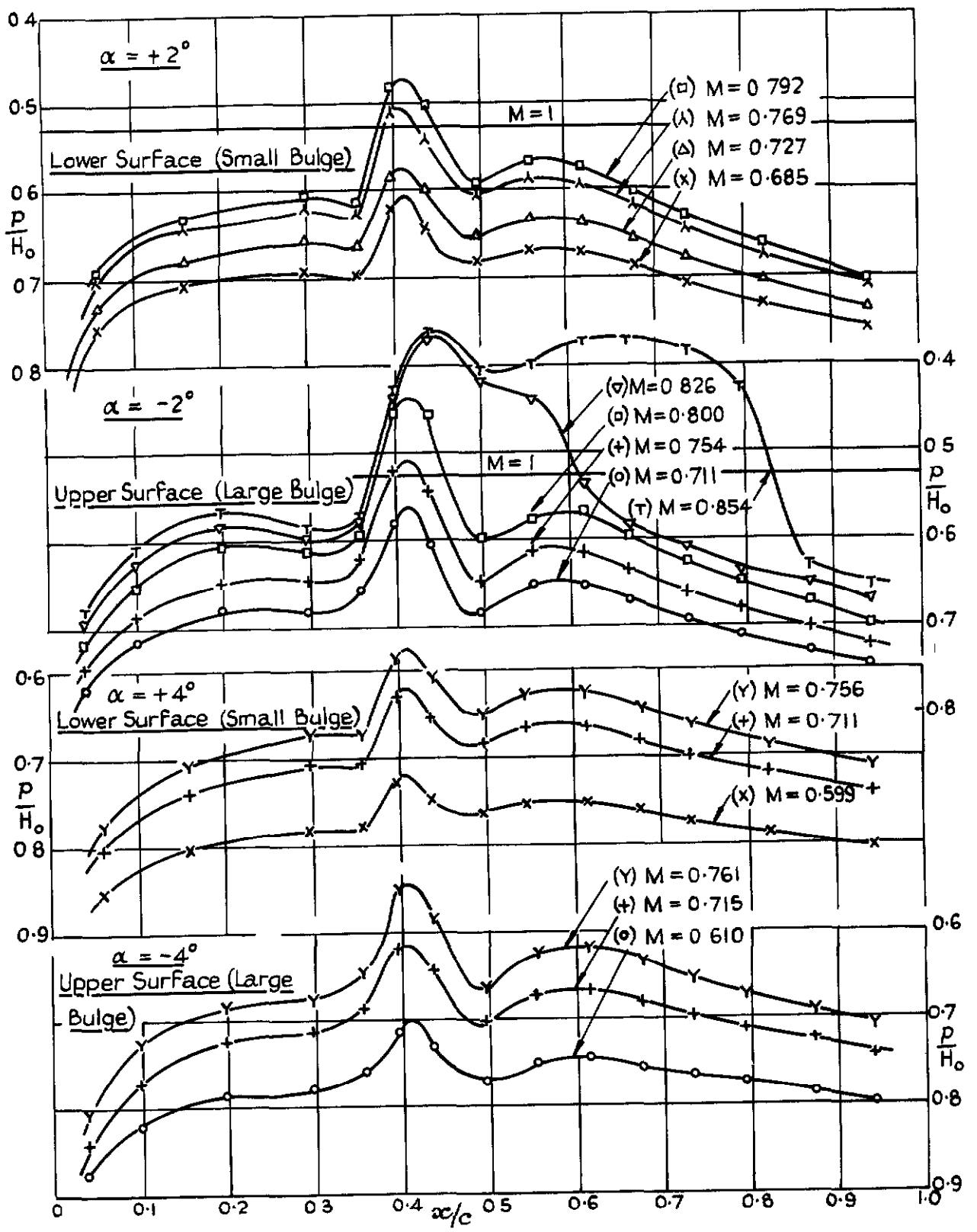

Pressure Distribution for Aerofoil with Bulges: $\alpha = \pm 2°, \pm 4°$.

E.E.M.

FIG. 7.

FIGS 7&8.

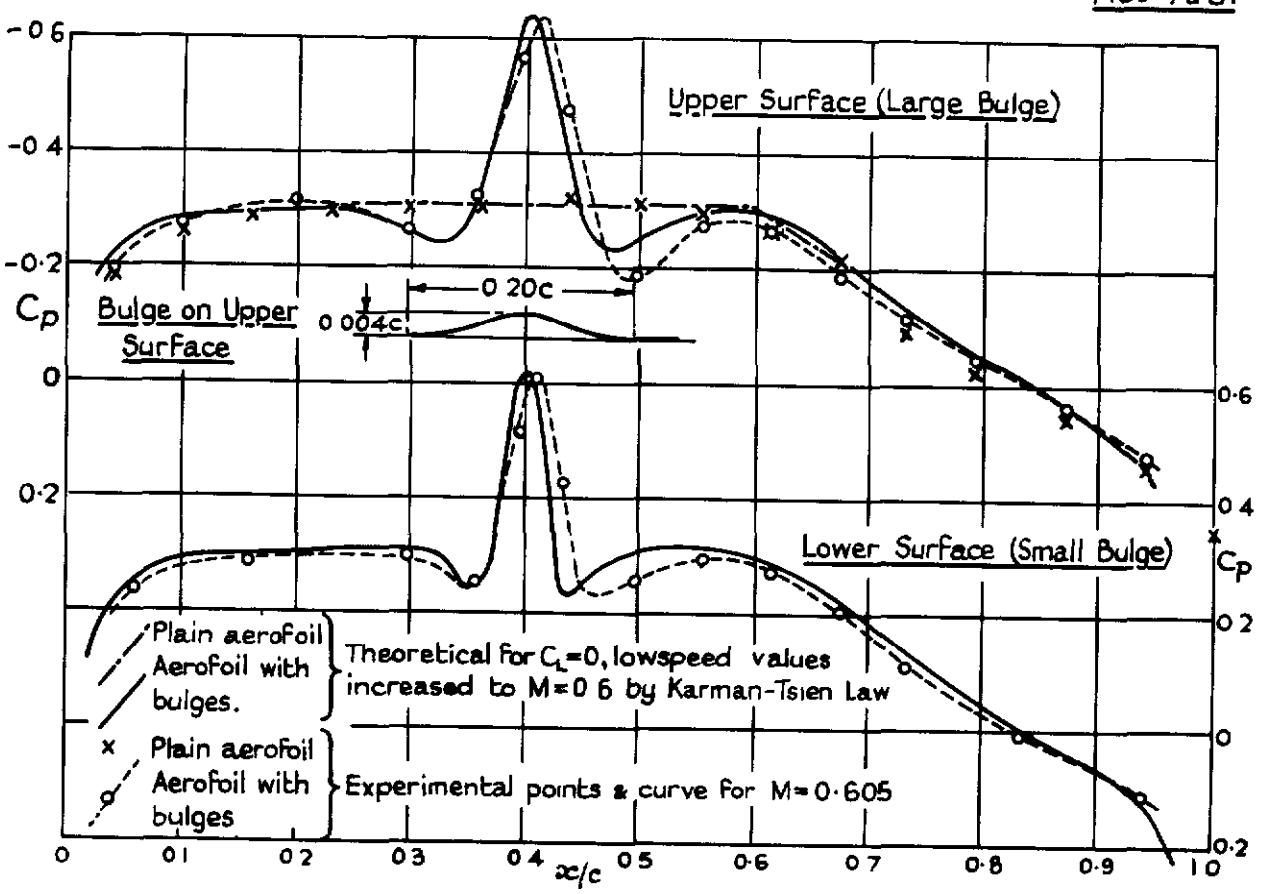

Comparison between Theoretical & Experimental Pressure Distributions

FIG. 8.

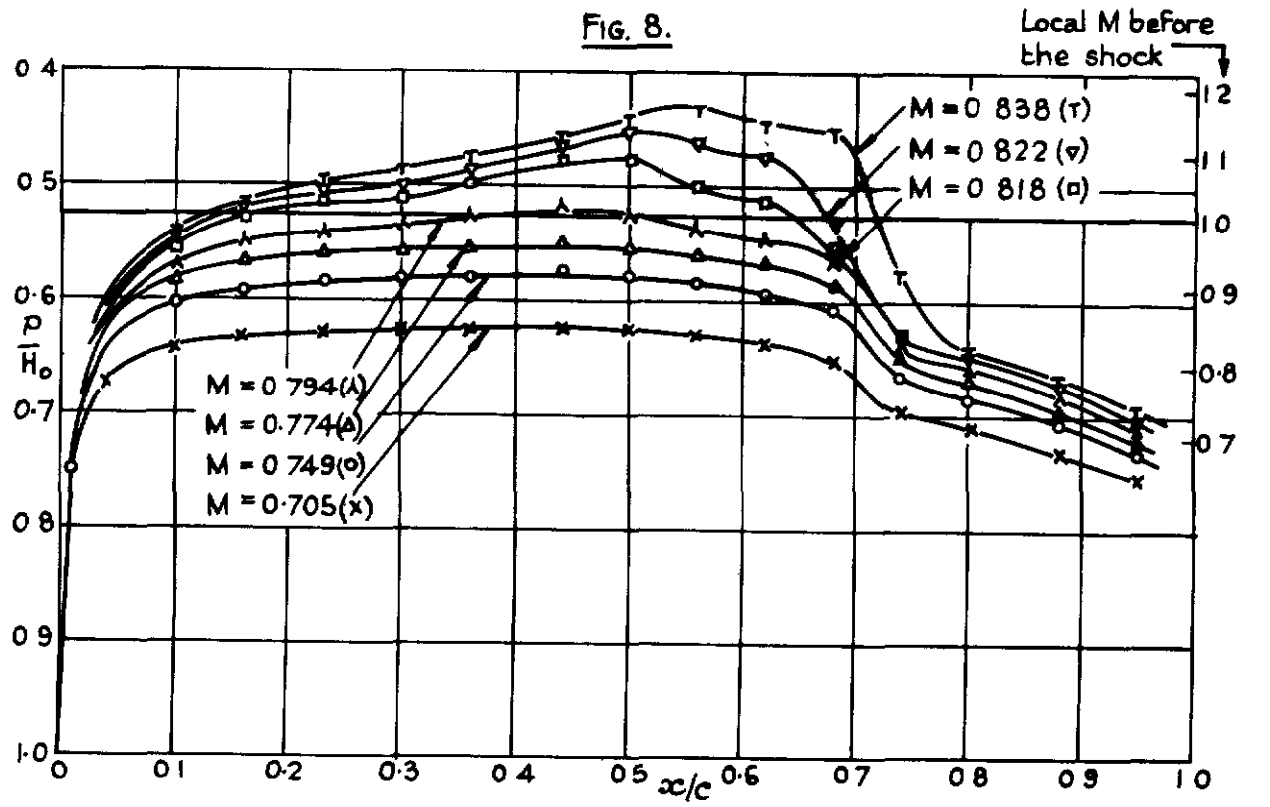

Pressure Distributions on the Plain Aerofoil $\alpha = 0°$

EEM

FIG. 9

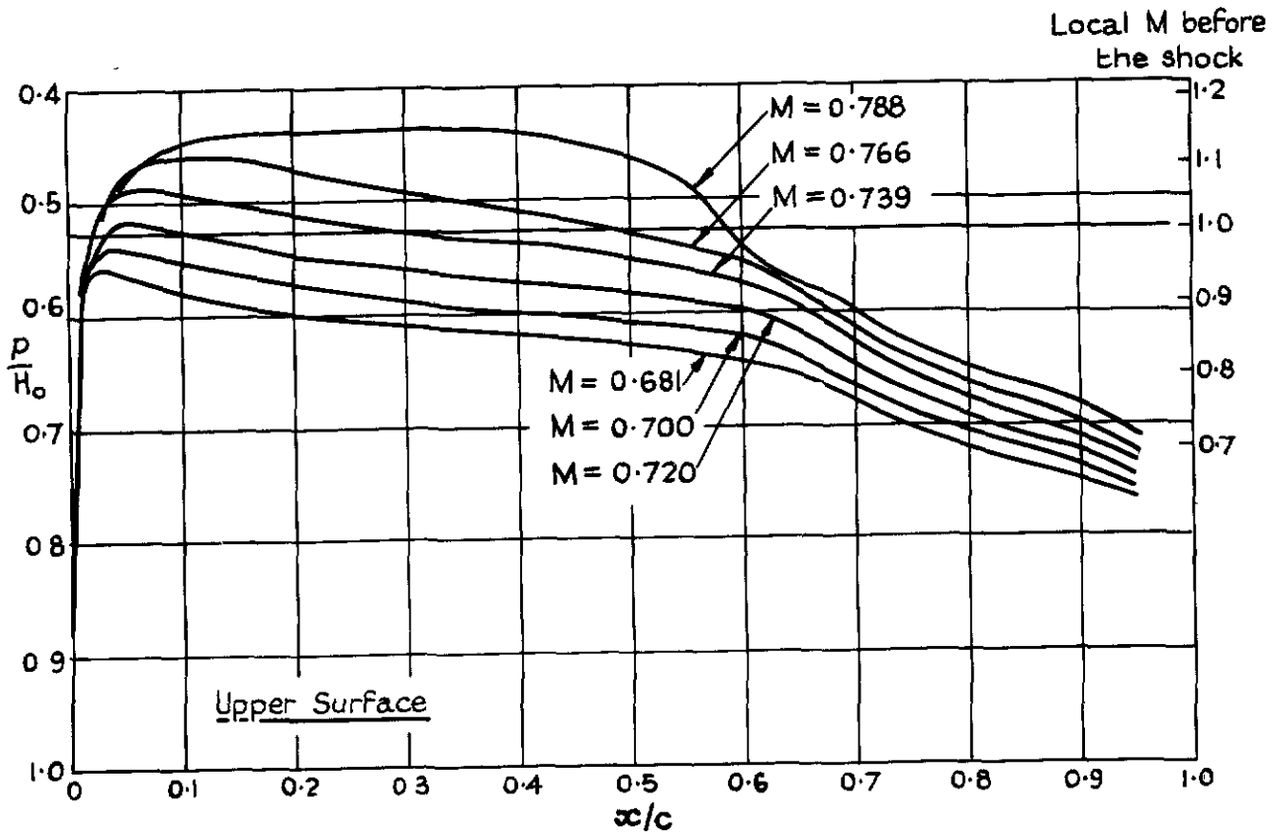

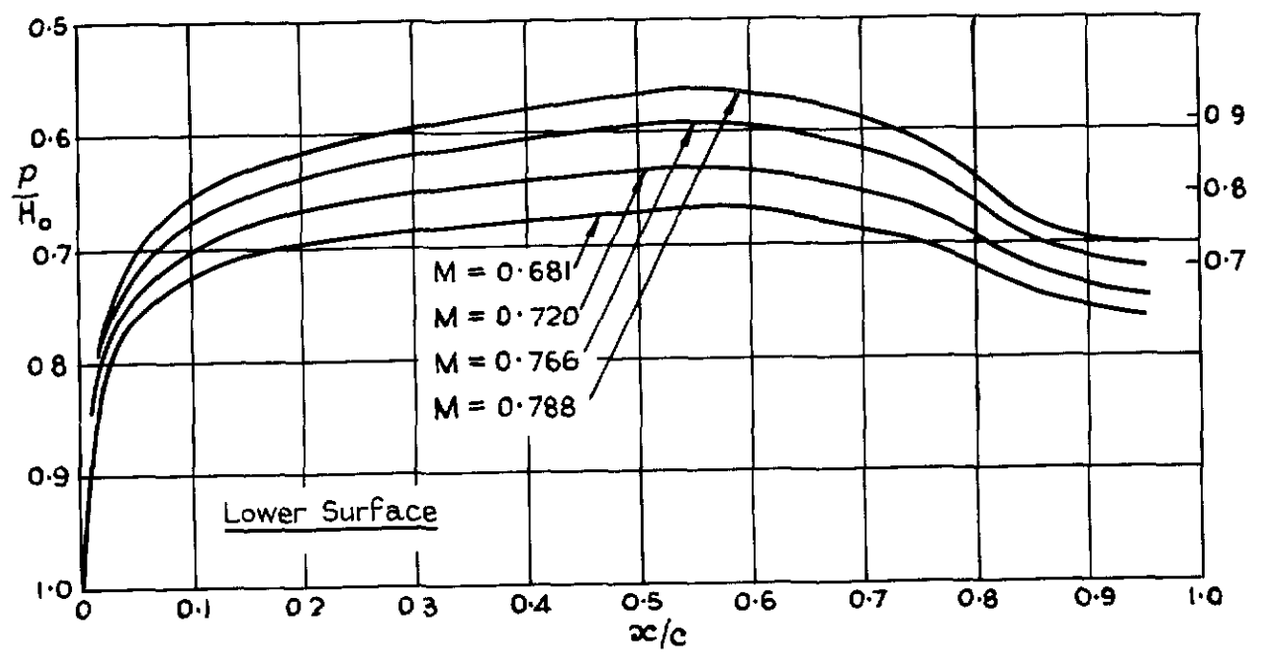

Pressure Distributions on the Plain Aerofoil $\alpha = 2°$.

EEM

FIG. 10

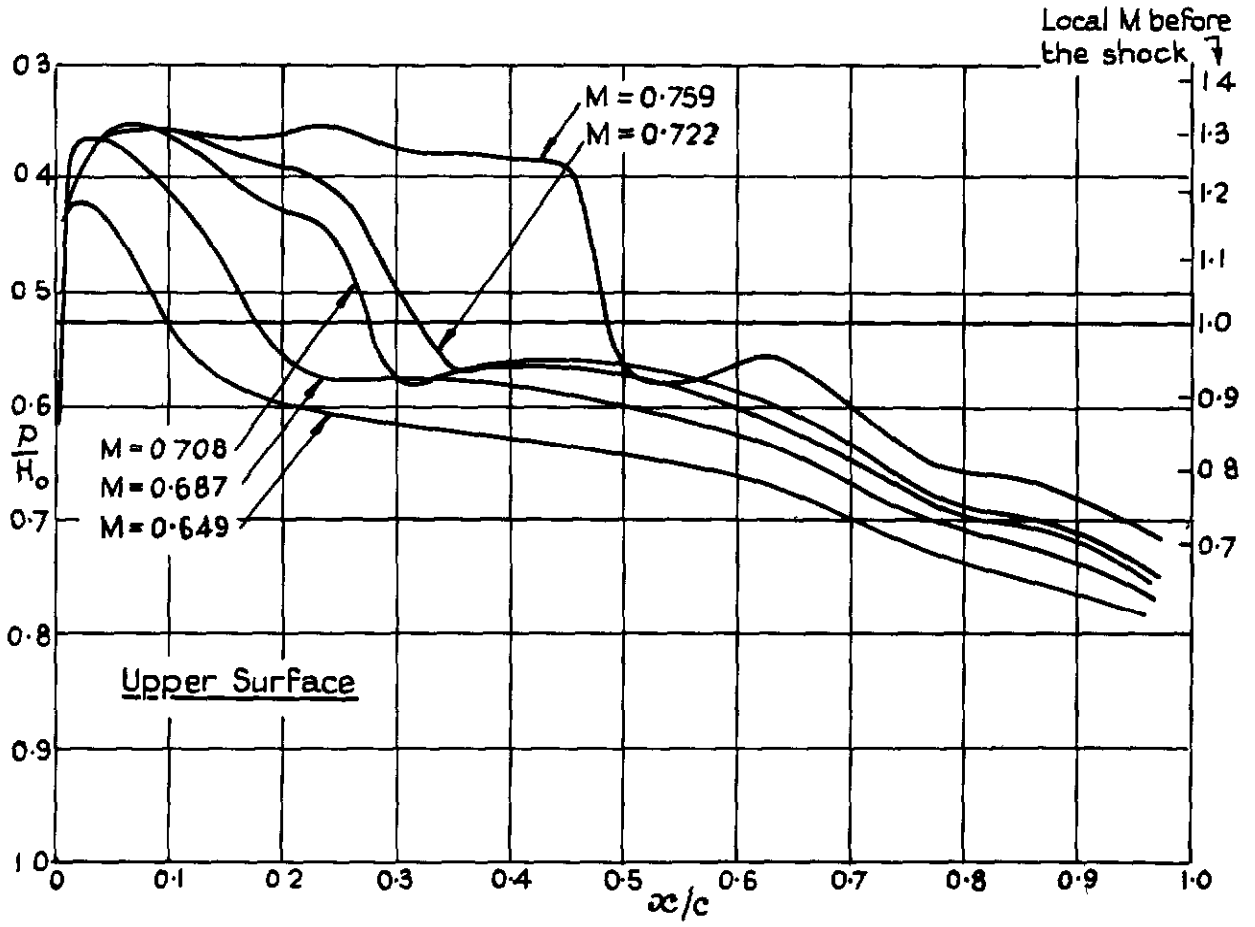

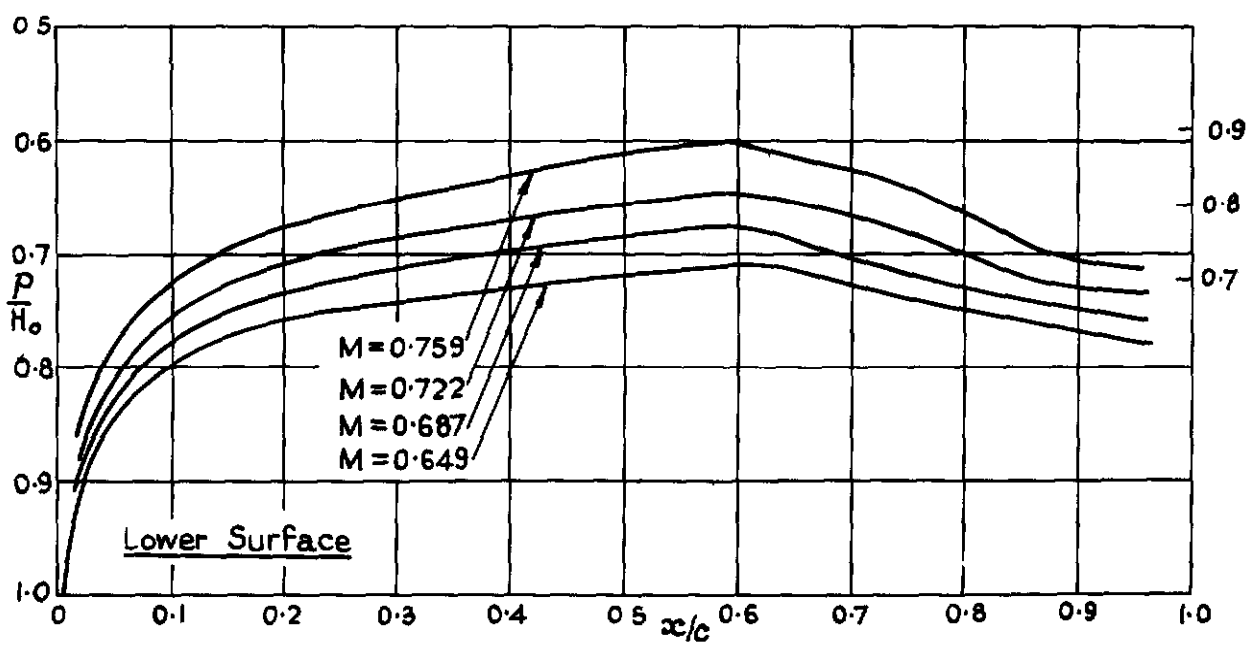

Pressure Distributions on the Plain Aerofoil: $\alpha = 4°$.

E.E.M.

FIG 11.

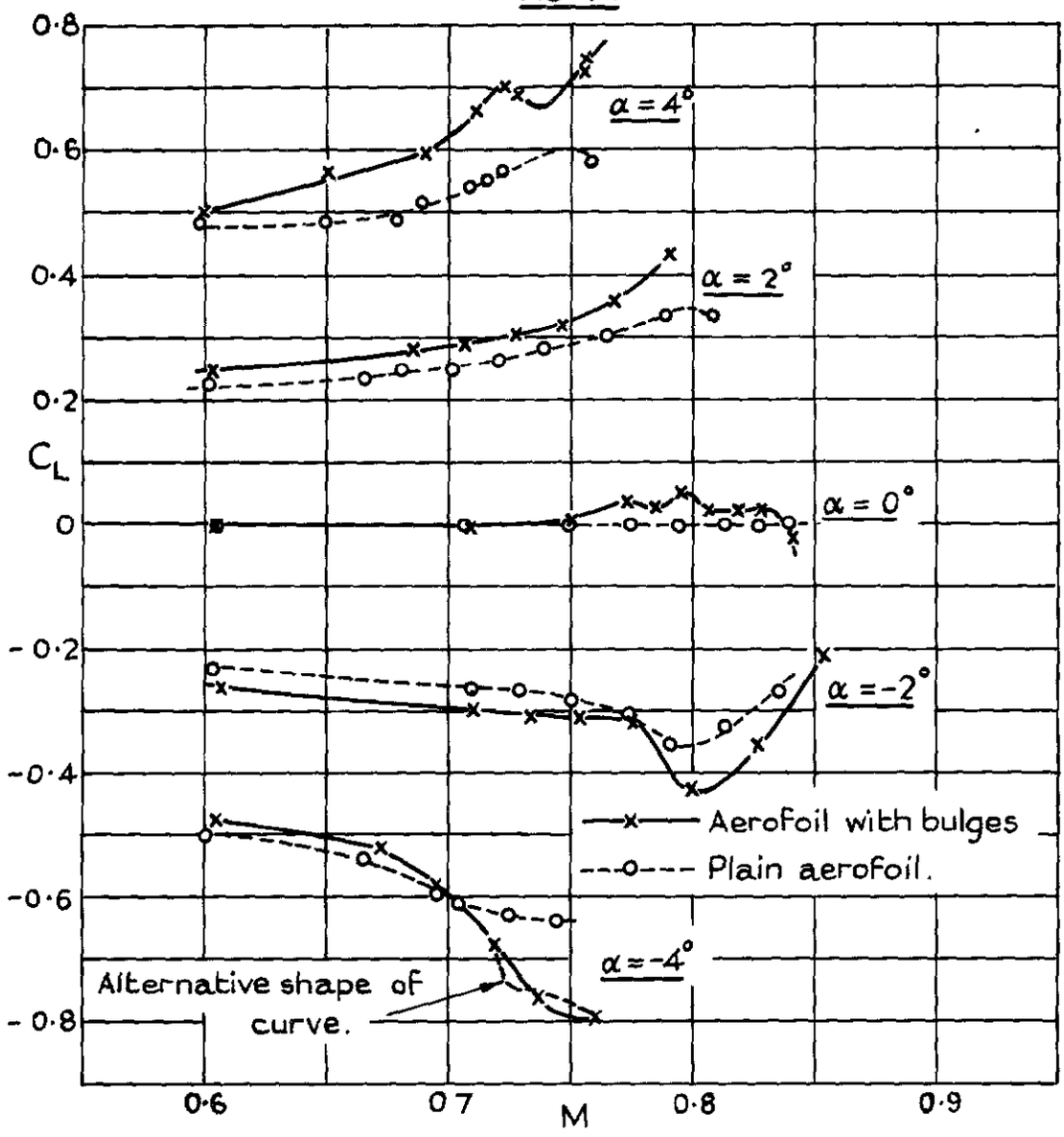

Variation of C_L with Mach Number for Aerofoil with & without Bulges.

FIG. 12a.

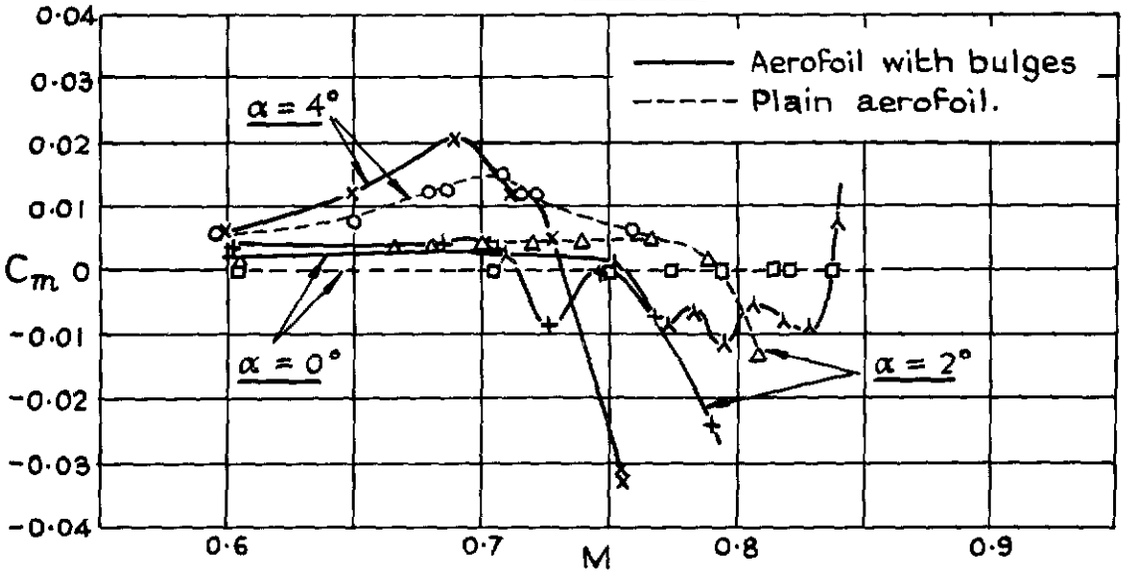

Comparison of C_m at Positive Incidences.

FIG. 12b

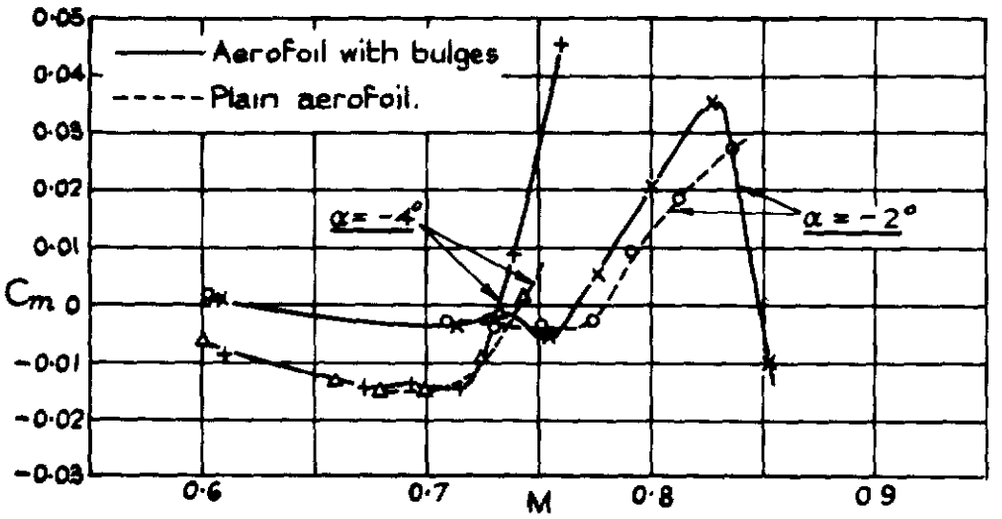

Comparison of C_m at Negative Incidences

FIG 13.

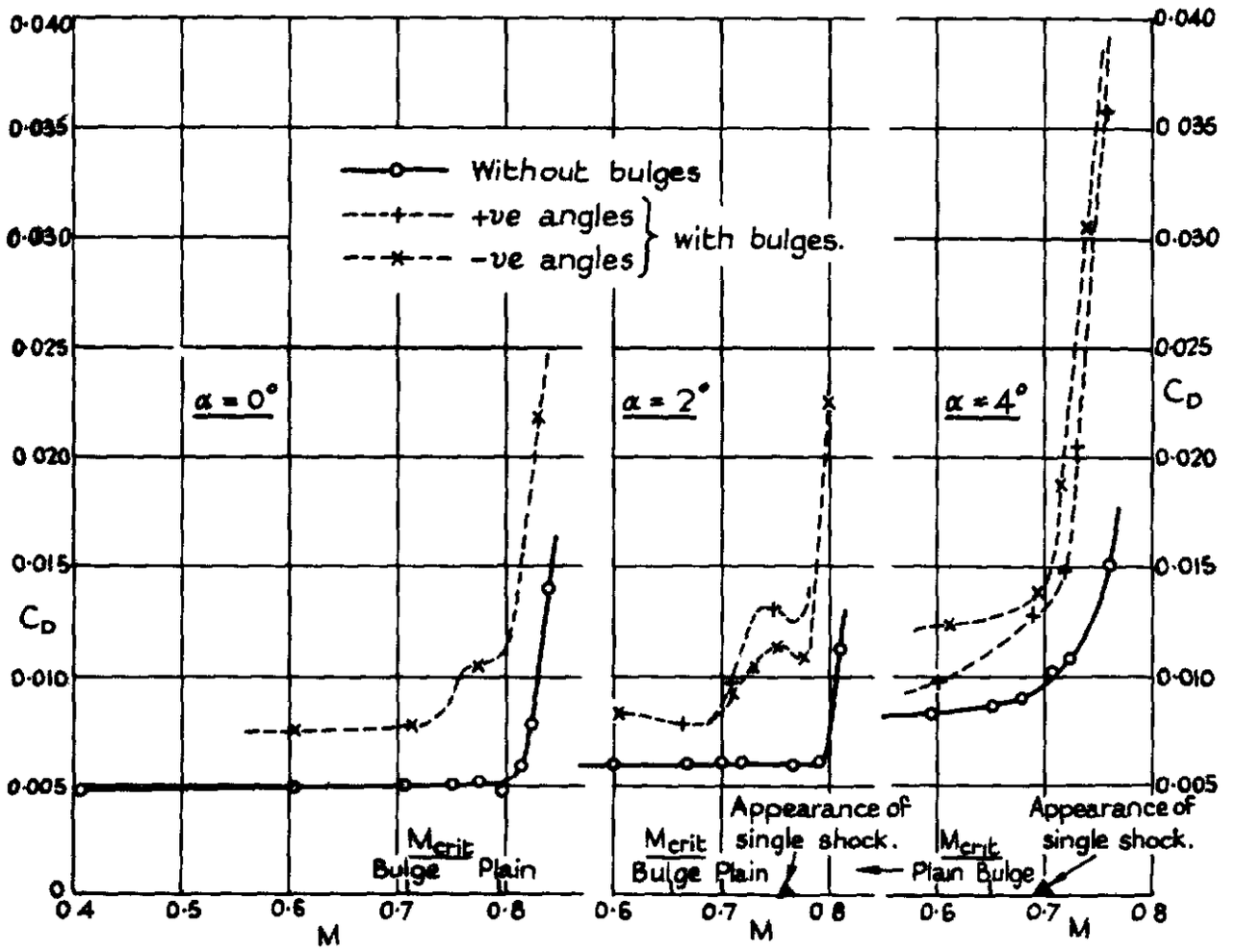

Comparison of C_D for Aerofoil with and without Bulges.

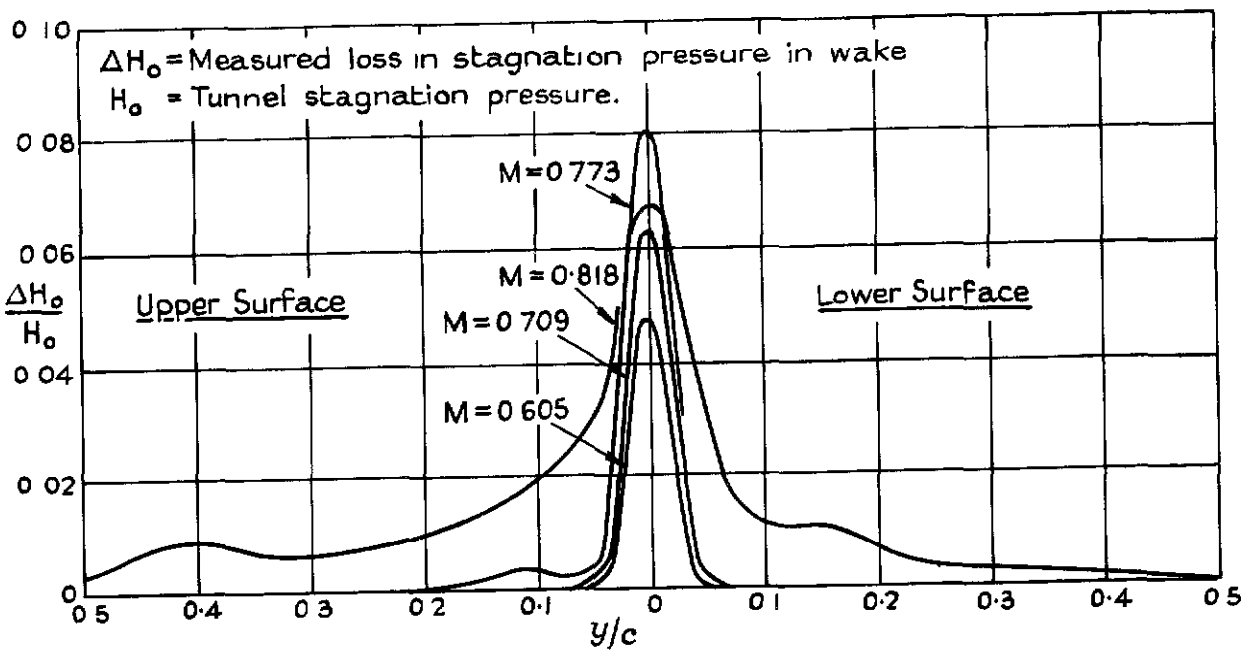

(a) Wake Traverse Curves at $\alpha = 0°$

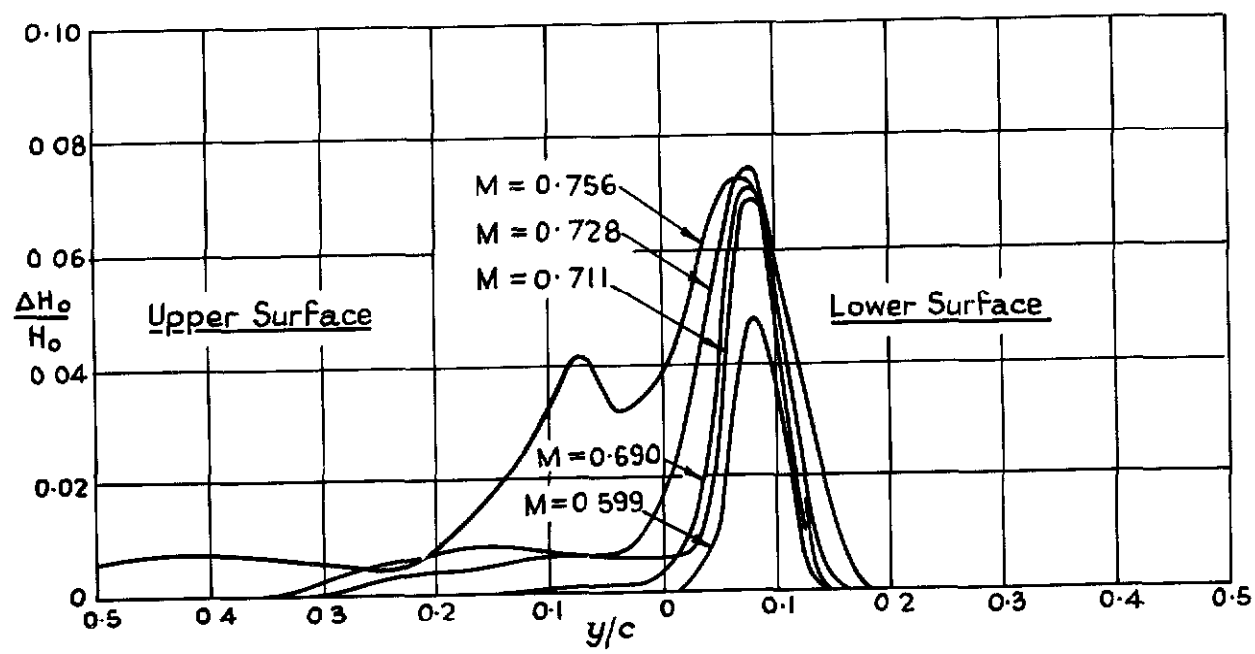

(b) Wake Traverse Curves at $\alpha = 4°$

Typical Wake Traverse Curves for Aerofoil with Bulges

EEM

Plain Aerofoil

Aerofoil with Bulges

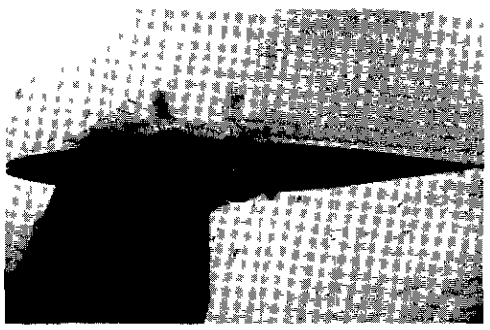

M = 0·749

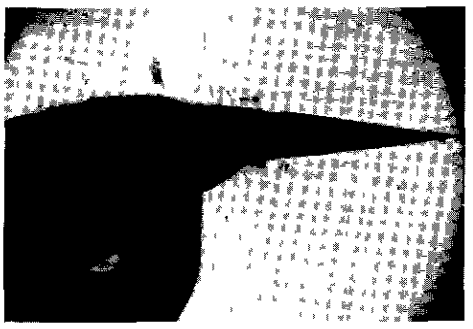

M = 0·751

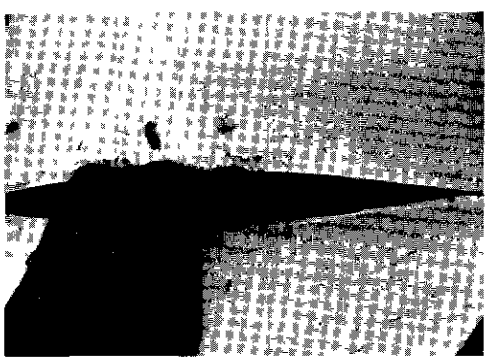

M = 0·774

M = 0·773

M = 0 794

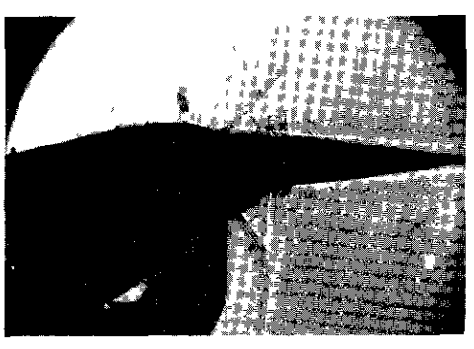

M = 0·795

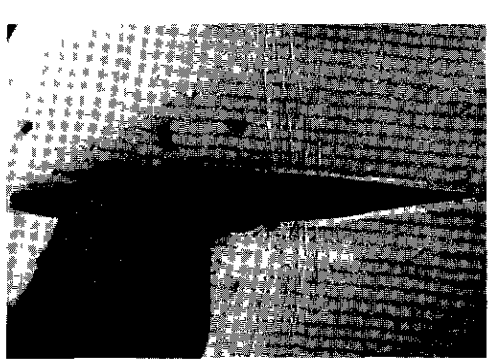

M = 0·818

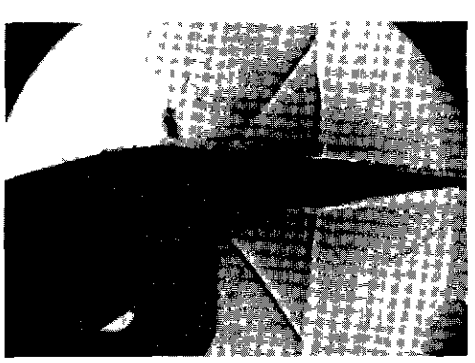

M = 0 818

Direct-shadow photographs of Flow around RAE 104 Aerofoil with and without bulges.

$\alpha = 0^{\circ}$

FIG. 15 b.

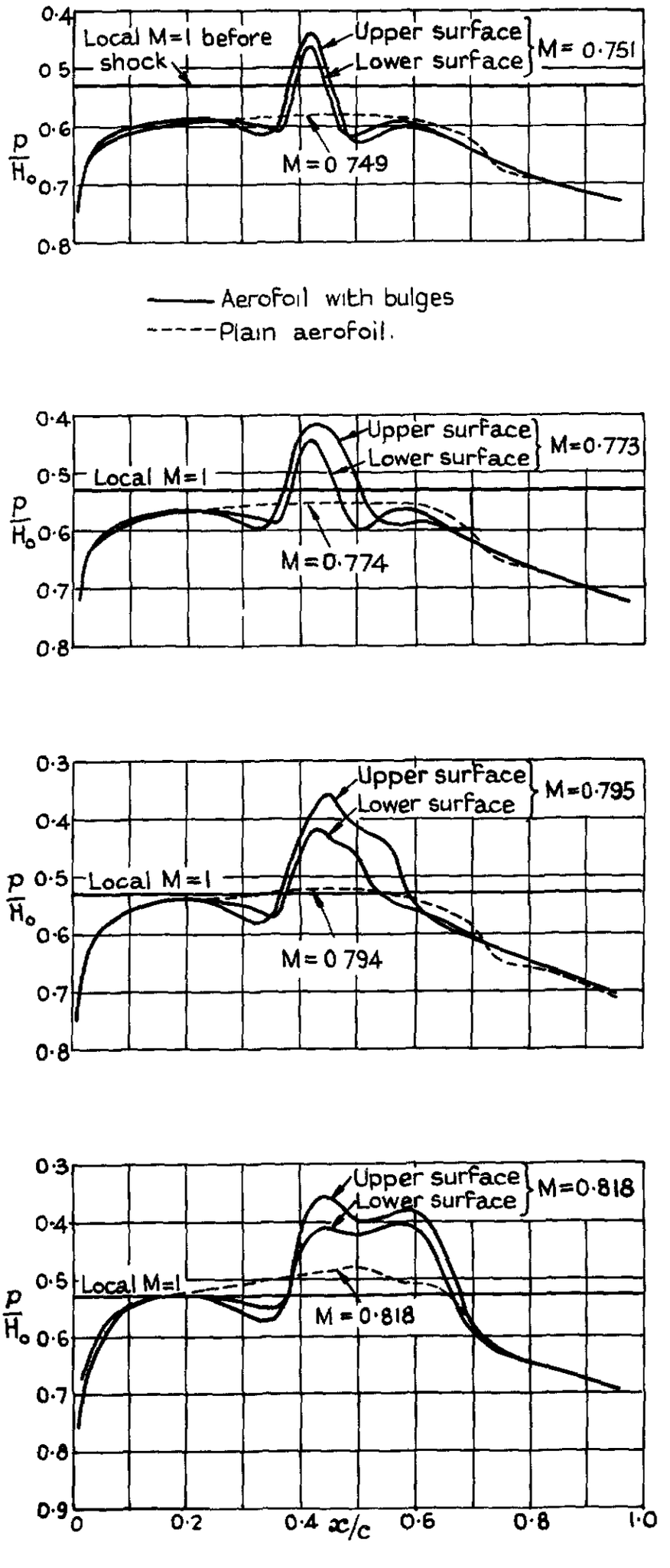

Comparison Pressure Distributions For $\alpha = 0°$

Plain Aerofoil

Aerofoil with Bulges

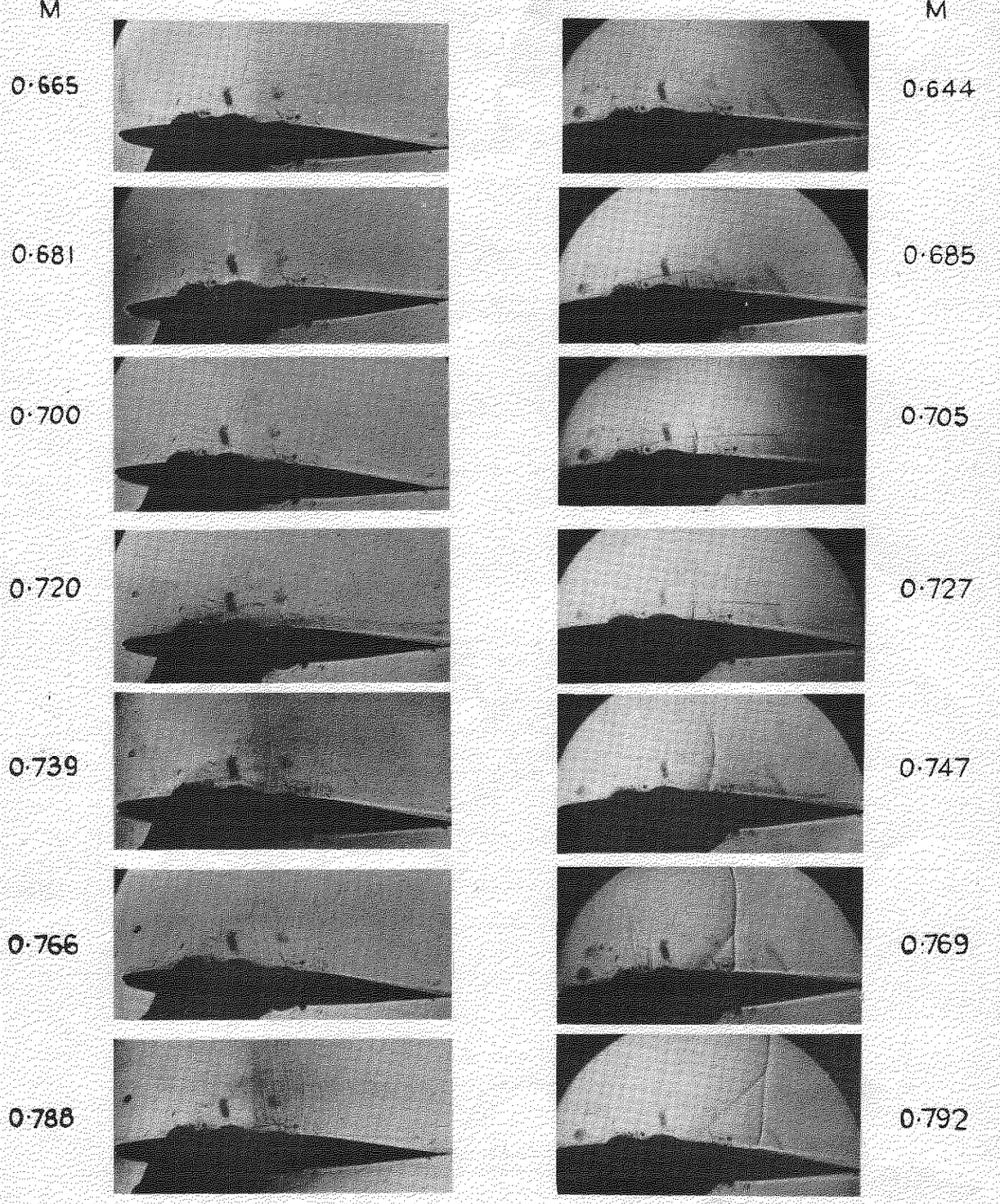

Direct-shadow photographs of flow around RAE 104 Aerofoil with and without bulges.

$\alpha = 2°$

Fig 16b.

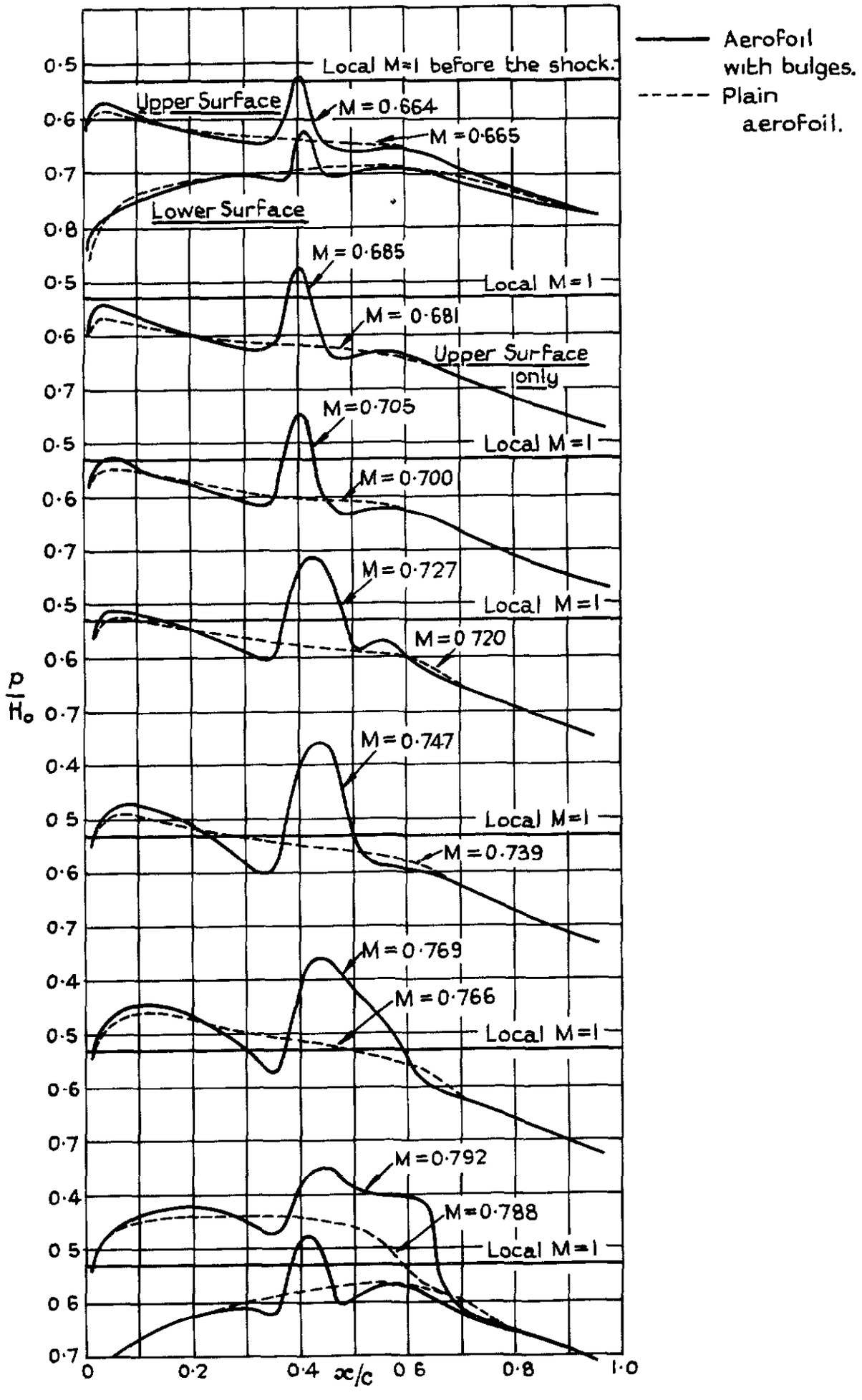

Comparison Pressure Distributions for $\alpha = 2°$.

FIG 15b.

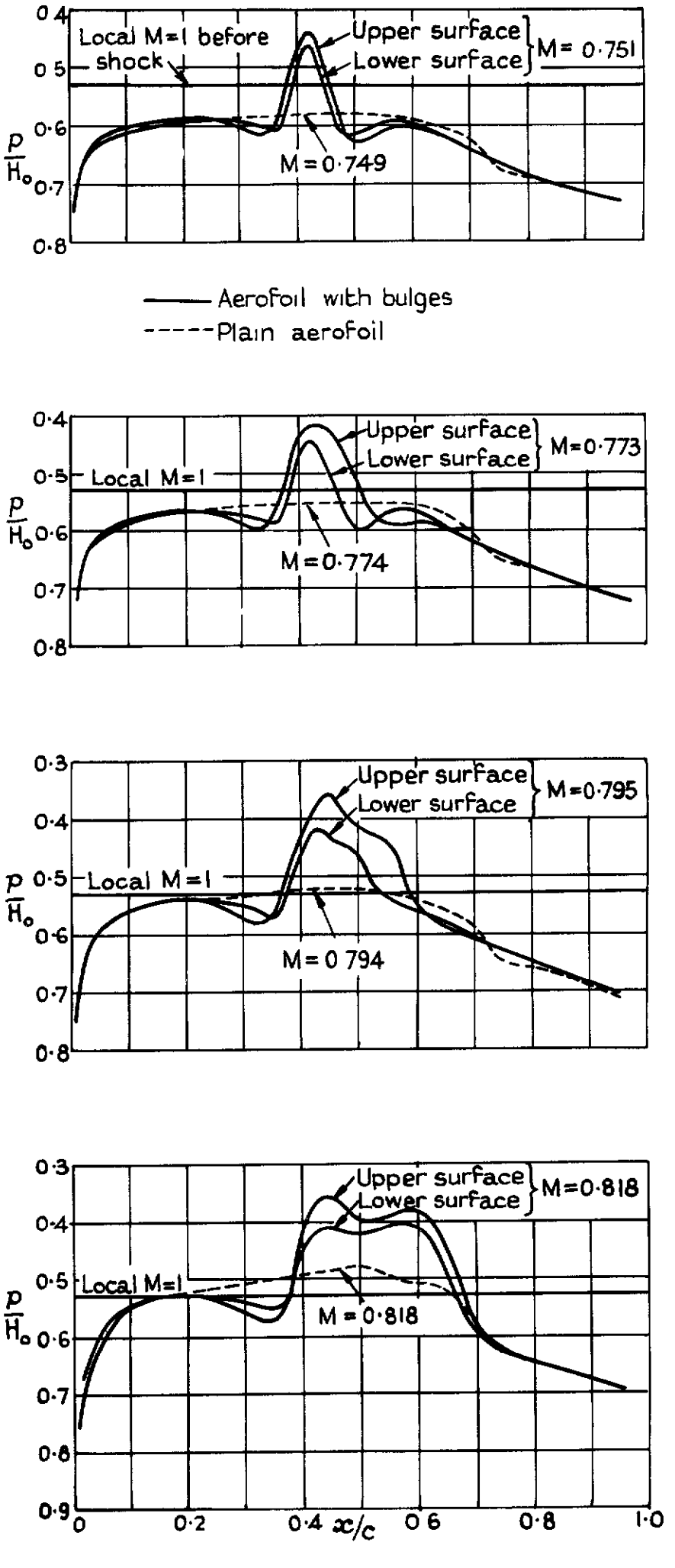

Comparison Pressure Distributions for $\alpha = 0°$.

Plain Aerofoil

Aerofoil with Bulges.

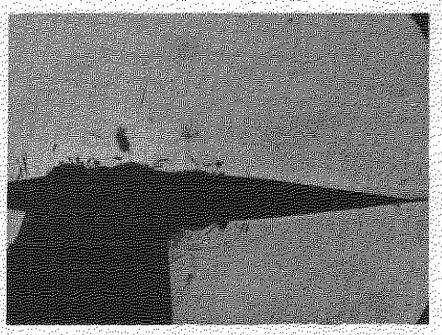

M = 0·649

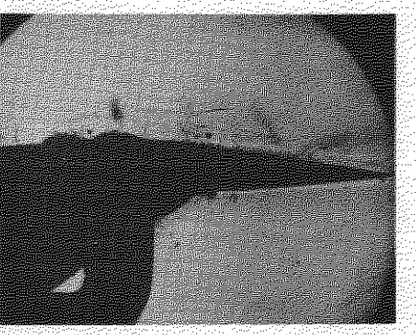

M = 0·650

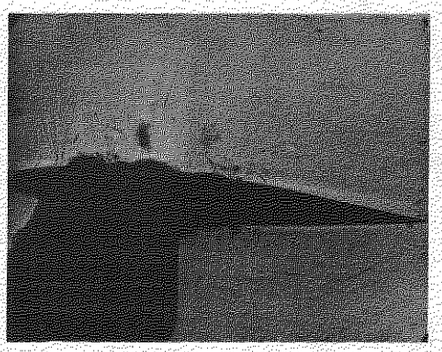

M = 0·687

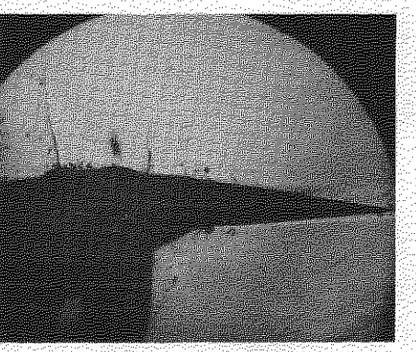

M = 0·690

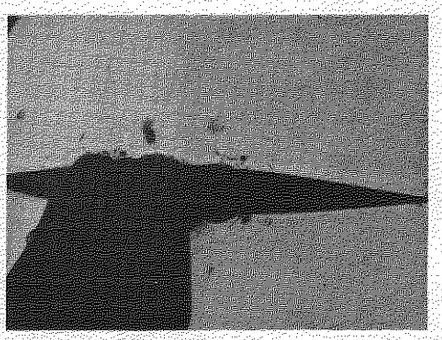

M = 0·722

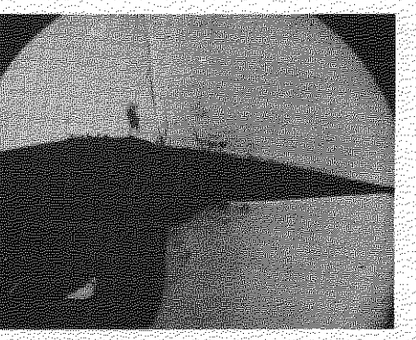

M = 0·717

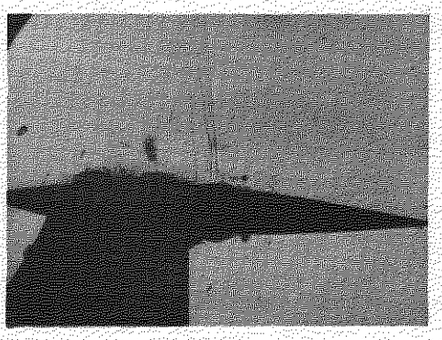

M = 0·759

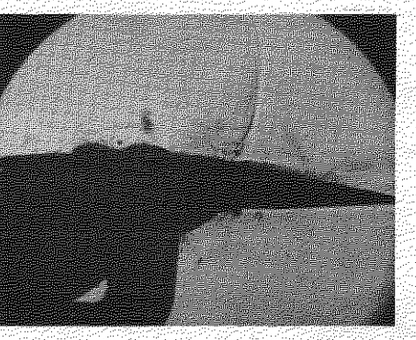

M = 0·756

Direct-shadow photographs of flow around RAE 104 Aerofoil with and without bulges.

$\alpha = 4°$.

FIG. 17b.

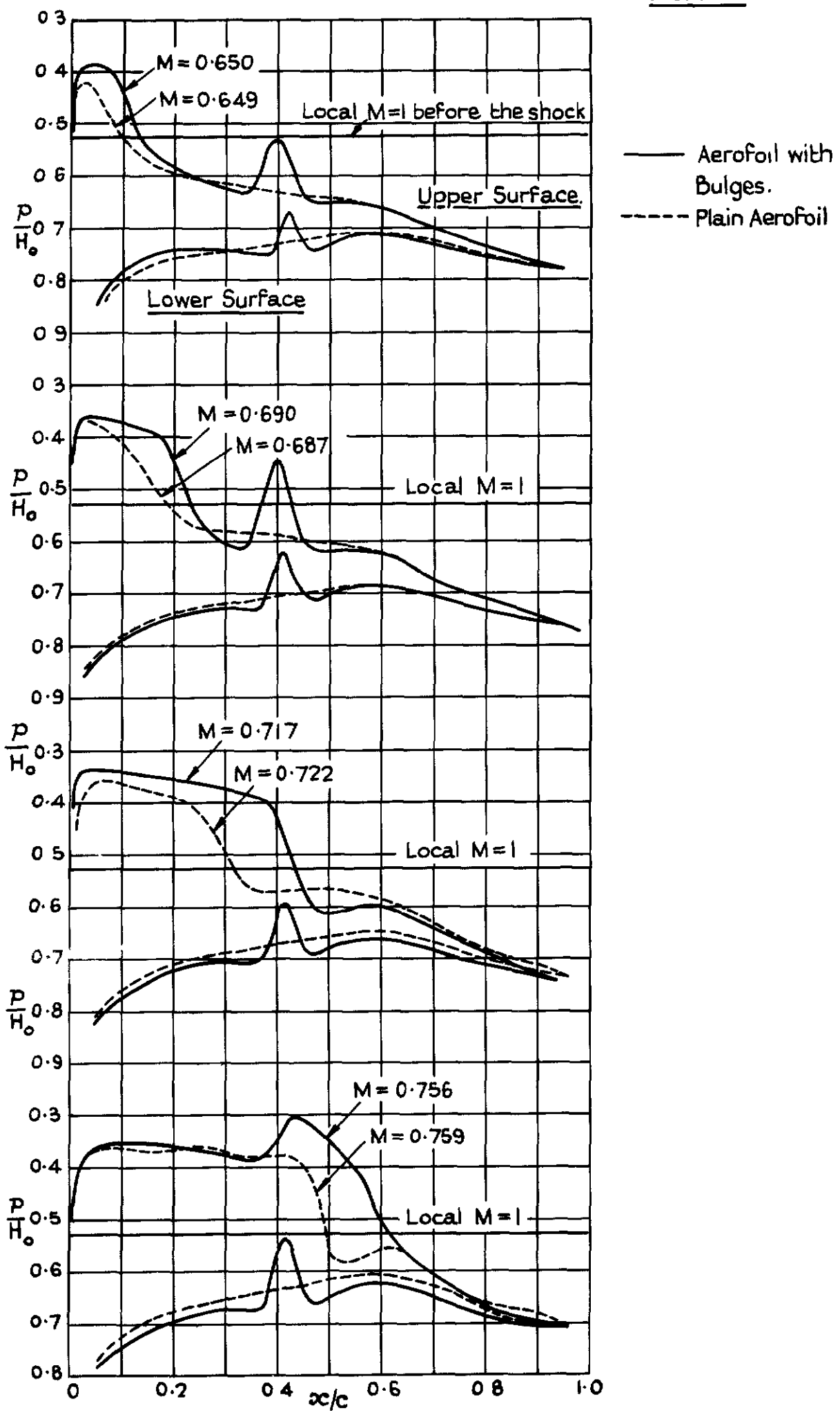

Comparison Pressure Distributions for $\alpha = 4^\circ$

Plain Aerofoil

Aerofoil with bulges.

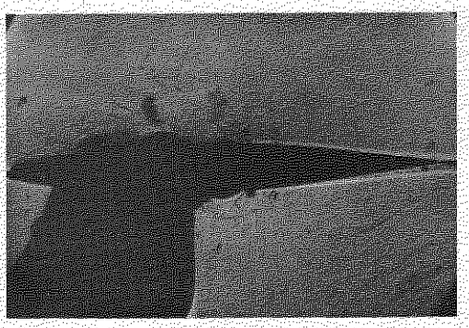

M = 0·709

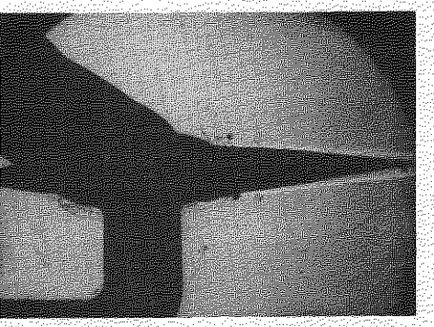

M = 0·711

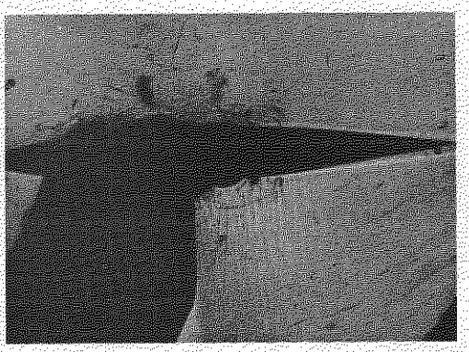

M = 0·751

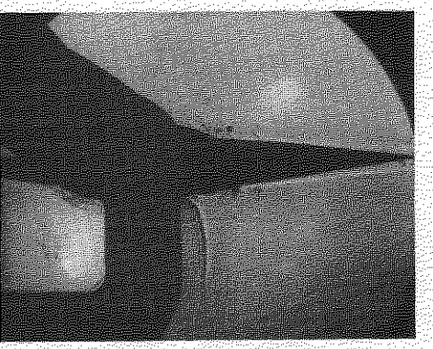

M = 0·754

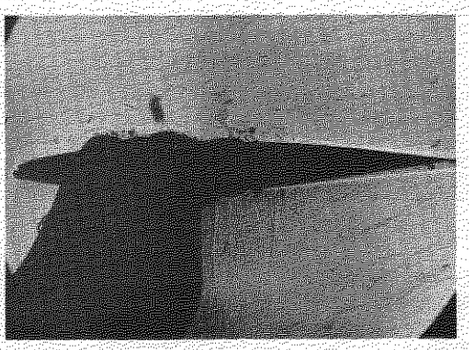

M = 0·774

M = 0·776

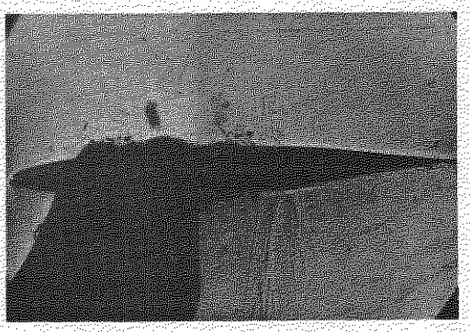

M = 0·791

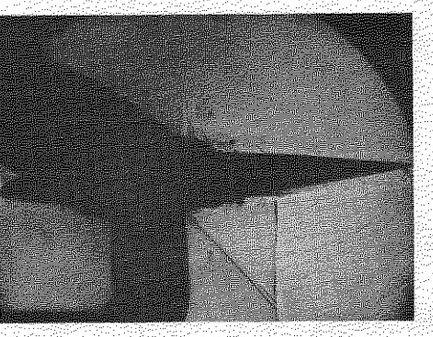

M = 0·800

Direct-shadow photographs of flow around RAE 104 Aerofoil with and without bulges.

$\alpha = -2°$

FIG. 18b.

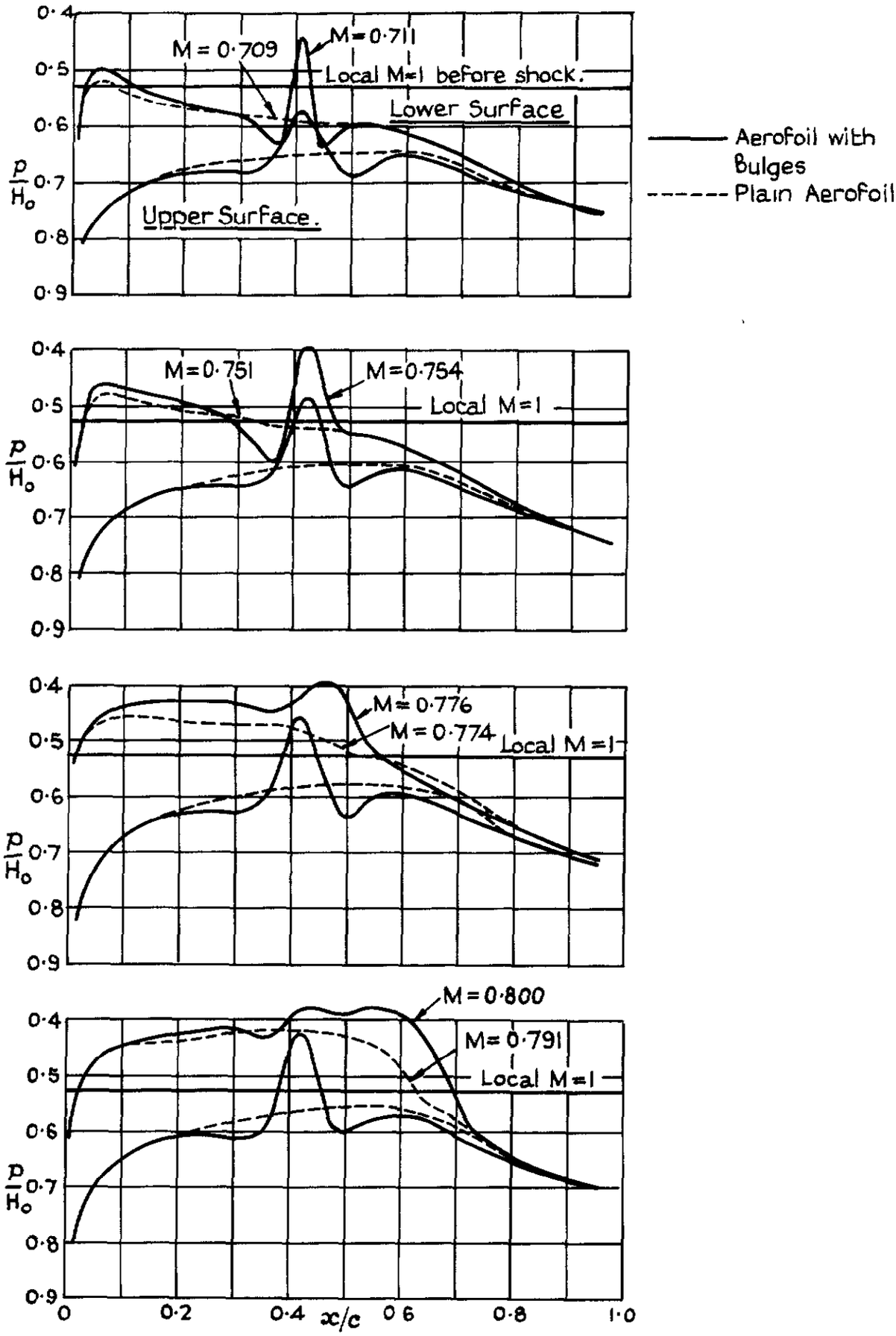

Comparison Pressure Distributions for $\alpha = -2°$

EEM

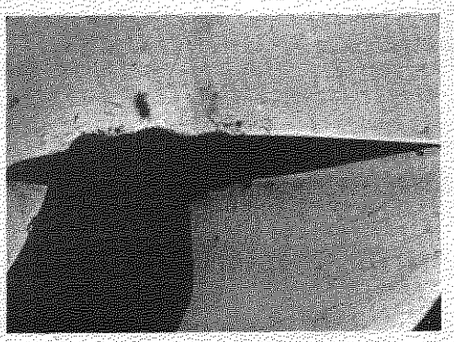

M = 0·683

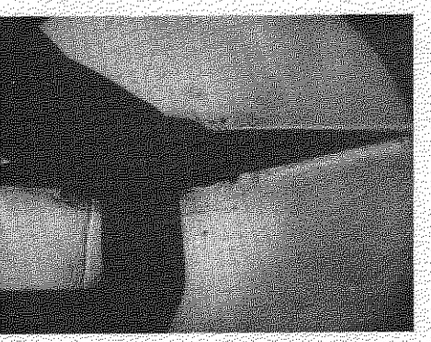

M = 0·694

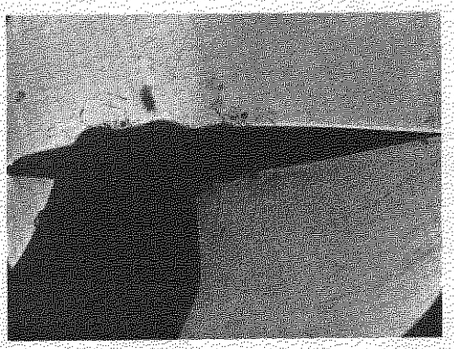

M = 0·724

No photograph

M = 0·715

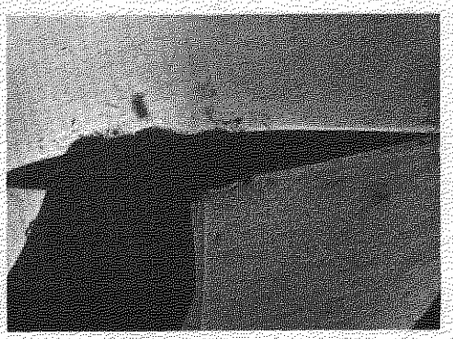

M = 744

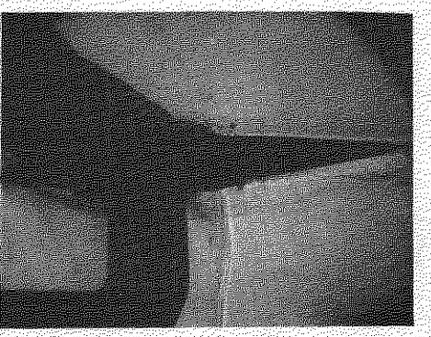

M = 0·738

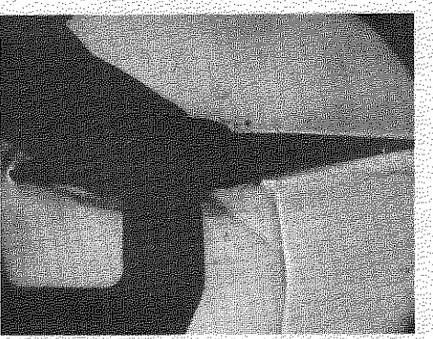

M = 0·761

Direct - shadow photographs of flow around RAE 104 Aerofoil with and without bulges.

$\alpha = -4°$

FIG. 19 b.

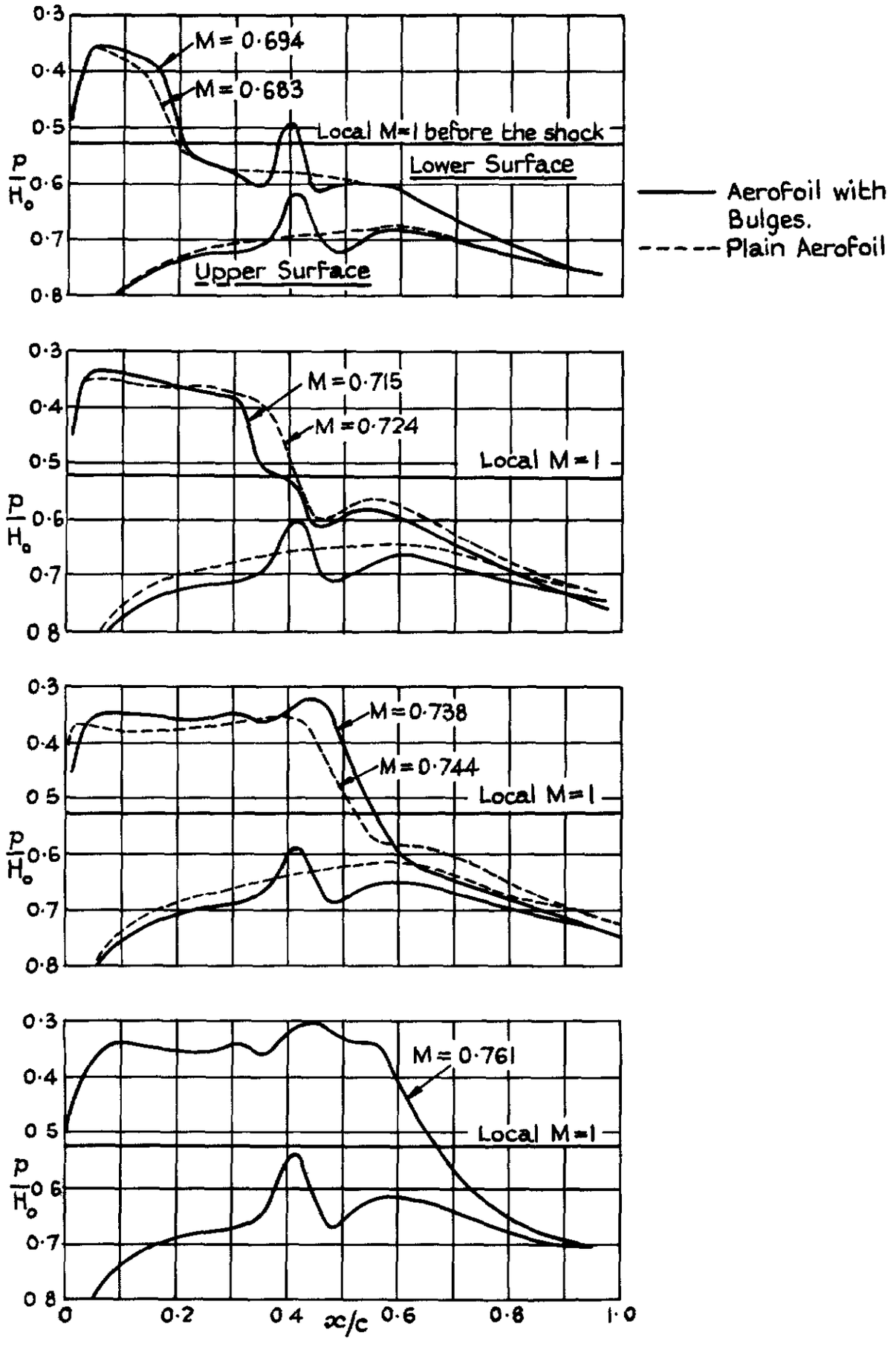

Comparison Pressure Distributions for $\alpha = -4°$.

FIG. 20.

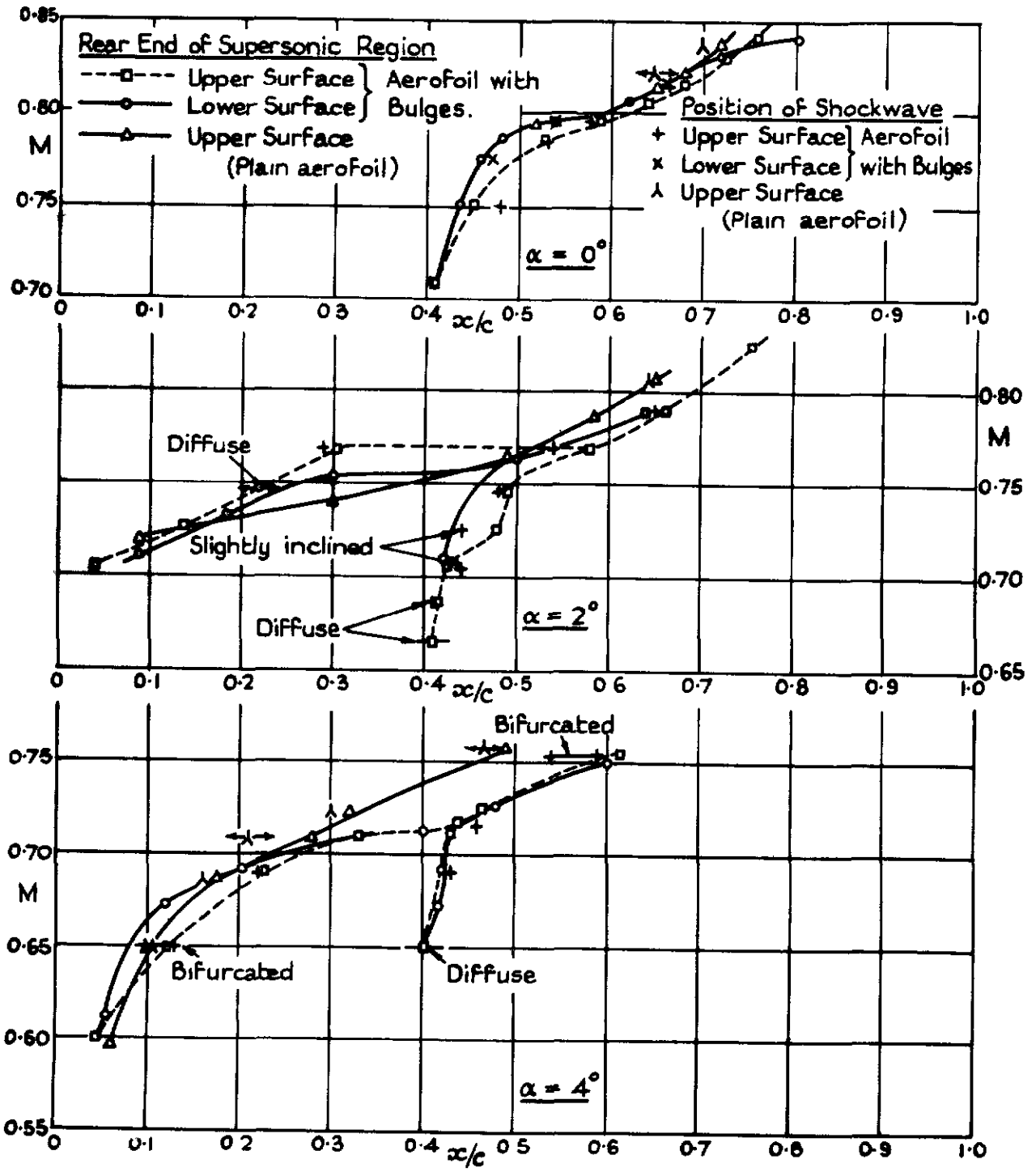

Position of Shockwave and Rear End of Supersonic Region.

EEM

DS 7873/1/K 3 2/52 CL

C P No. 78
(13,786)

A.R.C. Technical Report

PRINTED AND PUBLISHED BY HER MAJESTY'S STATIONERY OFFICE
To be purchased from
York House, Kingsway, LONDON, W C.2 429 Oxford Street, LONDON, W 1
P O Box 569, LONDON, S E 1
13a Castle Street, EDINBURGH, 2 1 St. Andrew's Crescent, CARDIFF
39 King Street, MANCHESTER, 2 Tower Lane, BRISTOL, 1
2 Edmund Street, BIRMINGHAM, 3 80 Chichester Street, BELFAST
or from any Bookseller
1952
Price 5s 0d net
PRINTED IN GREAT BRITAIN

DS 7873/3/K3 S O Code No. 23-9006-78